CHALMERS
UNIVERSITY OF TECHNOLOGY

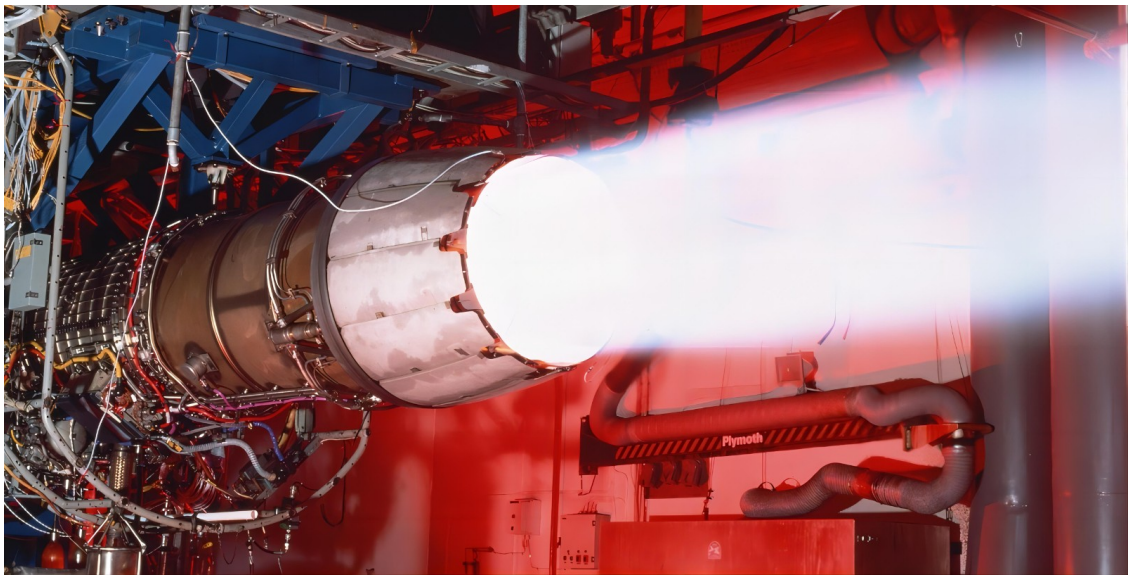

Modelling and Evaluation of Jet Engine Fuel System Designs

Master's thesis in Mobility Engineering

PER SAMUELSSON
HJALMAR STRÖMFELDT

DEPARTMENT OF MECHANICS AND MARITIME SCIENCES
CHALMERS UNIVERSITY OF TECHNOLOGY
Gothenburg, Sweden 2024
www.chalmers.se

Master's thesis 2024

Modelling and Evaluation of Jet Engine Fuel System Designs

PER SAMUELSSON
HJALMAR STRÖMFELDT

CHALMERS
UNIVERSITY OF TECHNOLOGY

Department of Mechanics and Maritime Sciences
Chalmers University of Technology
Gothenburg, Sweden 2024

Modelling and Evaluation of Jet Engine Fuel System Designs
PER SAMUELSSON
HJALMAR STRÖMFELDT

Supervisor: Niklas Kringstad, GKN Aerospace Sweden AB
Examiner: Professor Tomas Grönstedt, Mechanics and Maritime Sciences

Master's Thesis 2024
Department of Mechanics and Maritime Sciences
Chalmers University of Technology
SE-412 96 Gothenburg
Telephone +46 31 772 1000

Cover: RM12 engine test, used with permission from GKN Aerospace Sweden AB

Typeset in LaTeX
Gothenburg, Sweden 2024

Modelling and Evaluation of Jet Engine Fuel System Designs
PER SAMUELSSON
HJALMAR STRÖMFELDT
Department of Mechanics and Maritime Sciences
Chalmers University of Technology

Abstract

This master thesis investigates the main fuel pump of the RM12 engine used in the JAS 39 Gripen C/D fighter jet, with the aim of identifying and modelling the main fuel pump as well as alternative fuel system configurations. The purpose of this project is to understand performance, efficiency, and limitations of the current fuel system, as well as to explore potential improvements using alternative fuel systems and pump architectures. By combining publicly available data, data from uninstalled accessory rig tests, as well as data from uninstalled engine tests, the system model compares the performance of different fuel systems at different steady state operating conditions. The system model predicts pump power usage and fuel heat sink capability among other parameters. These performance parameters have a direct impact on aircraft performance and provide insight in design and optimization of future jet engine fuel systems. The results indicates that a variable displacement main fuel pump or an electrically driven variable speed main fuel pump may be well suited with regards to minimizing power extraction and added heat to the fuel. Further studies of these configurations may therefore be of interest.

Keywords: RM12, pumps, fuel system, main fuel pump, jet engine, afterburner

Acknowledgements

We would like to express a special thanks our supervisor Niklas Kringstad at GKN Aerospace for his guidance and advice throughout the creation of this thesis.

We also acknowledge Victor Isidorsson and the rest of division 7162 at GKN Aerospace for their openness and kindness towards us.

Thanks to Mikael Stribrand and Johan Öhman for providing insights on the test rig specifications, and to Eric and Pernilla for carrying out our custom rig test.

Chalmers Library and Jonathan Mårtensson are acknowledged for providing articles and books that have been essential for the literature study.

We thank Michael Crona and Simon Dinger for their thorough review and feedback.

Lastly, we acknowledge Tomas Grönstedt for taking on the role as examiner for our thesis.

Per Samuelsson & Hjalmar Strömfeldt, Gothenburg, June 2024

List of Acronyms

Below is the list of acronyms that have been used throughout this thesis listed in alphabetical order:

ABC	Afterburner Fuel Control
ABP	Afterburner Fuel Pump
AGB	Accessory Gear Box
A/B	Afterburner
A/C	Aircraft
BEP	Best Efficiency Point
CFD	Computational Fluid Dynamics
FADEC	Full Authority Digital Engine Control
FI	Flight Idle
HP	High Pressure
IRP	Intermediate Rated Power
LP	Low Pressure
MFC	Main Fuel Control
MFP	Main Fuel Pump
MT	Maximum A/B Thrust
NH	Rotational Speed of the High Pressure Rotor
$NPSH_r$	Required Net Positive Suction Head
RPM	Rotations Per Minute
SFC	Specific Fuel Consumption
WFM	Weighted Fuel Main
WFR	Weighted Fuel Reheat
w/o	Without

Nomenclature

Below is the nomenclature of parameters that have been used throughout this thesis.

Parameters

A	Area [m^2]
C_d	Discharge coefficient [-]
c_p	Specific heat capacity [J/(kg· K)]
D	Diameter [m]
d_s	Specific diameter [-]
g	Gravitational acceleration constant [m/s^2]
H	Head [m]
h	Specific enthalpy [J/kg]
$\dot{m}$	Mass flow [kg/s]
Ma	Mach number [-]
n_q	Specific speed [$m^{3/4}/(min{\cdot}\sqrt{s})$]
p	Pressure [Pa]
Q	Volume flow [m^3/s]
q^*	Normalized volumetric flow rate [-]
$\dot{Q}$	Heat power [J/s]
Re	Reynolds number [-]
U	Sliding velocity [-]
u	Internal energy [J/kg]
V	Mean flow velocity [m/s]
V	Specific volume [m^3/kg]
V_d	Displacement volume [m^3/s]
$\dot{W}_s$	Shaft power [J/s]
$\dot{W}_v$	Viscous power [J/s]

$\dot{w}_s$	Shaft work [J/kg]
α	Swash plate angle [-]
ΔH	Total dynamic head [m]
η	Efficiency [-]
η_m	Mechanical efficiency [-]
η_v	Volumetric efficiency [-]
μ	Dynamic viscosity [Pa· s]
μ_{JT}	Joule-Thomson coefficient [° C/Pa]
ϕ	Flow coefficient [-]
ψ	Head coefficient [-]
ρ	Density [kg/m^3]
ω	Pump shaft rotational speed [rad/s]
ω_s	Specific speed [-]

Contents

List of Acronyms **ix**

Nomenclature **xi**

List of Figures **xvii**

List of Tables **xix**

1 Introduction **1**
1.1 Background . . . 1
1.2 Aim . . . 2
1.3 Limitations . . . 3
1.4 Specification of the issue being investigated . . . 4

2 Theory **5**
2.1 Fuel system overview . . . 5
2.1.1 Aircraft booster pump . . . 5
2.1.2 Main fuel pump . . . 5
2.1.2.1 Pumping stages and fuel filter . . . 6
2.1.2.2 Main fuel control, bypass and servo flow . . . 6
2.1.3 A/B fuel pump and A/B fuel control . . . 8
2.1.4 Oil cooler . . . 8
2.1.5 Full authority digital engine control . . . 8
2.2 Pump and system curves . . . 8
2.2.1 Definition of head . . . 8
2.2.2 Pump efficiency . . . 9
2.2.3 Pump curves . . . 11
2.2.4 System curve . . . 11
2.2.5 System performance . . . 13
2.3 Dimensionless performance parameters . . . 13
2.3.1 Head and flow coefficients . . . 13
2.3.2 Specific speed and specific diameter . . . 14
2.3.3 Stribeck curve correlations for positive displacement pumps . . . 15
2.4 Pump type theory . . . 16
2.4.1 Specific diameter vs. specific speed diagrams . . . 16
2.4.2 Pump type descriptions . . . 16
2.4.2.1 Pump type classifications . . . 17

2.4.2.2 External gear pump . . . 18
2.4.2.3 Axial swash plate piston pump . . . 19
2.4.2.4 Radial centrifugal pump . . . 20
2.4.2.5 Partial emission pump . . . 21
2.5 Flow rate control methods . . . 23
2.5.1 Flow control by recirculation . . . 24
2.5.2 Flow control by variable displacement . . . 24
2.5.3 Flow control by throttling . . . 24
2.5.4 Speed flow control . . . 25
2.6 Fuel properties . . . 25
2.6.1 Density, viscosity and specific heat capacity . . . 25
2.6.2 Joule-Thomson coefficient . . . 25

3 Methods **27**
3.1 Estimation of density, viscosity and specific heat capacity . . . 27
3.2 Selection of model inputs . . . 28
3.3 Data collection . . . 29
3.3.1 Test rig description . . . 29
3.3.2 Formulation of test matrix . . . 29
3.3.3 Description of collected data . . . 31
3.4 Identification of Joule-Thomson coefficient . . . 32
3.5 Identification of LP stage head and efficiency curve . . . 32
3.6 Identification of HP stage volumetric efficiency . . . 33
3.7 RM12 state estimator formulation . . . 34
3.7.1 Calibration of model using HP total efficiency . . . 34
3.8 Selection and implementation of alternative MFP architectures . . . 36
3.8.1 System with centrifugal HP stage pump . . . 36
3.8.2 System with axial piston HP stage pump . . . 38
3.8.3 Electrically driven system with centrifugal stages . . . 39

4 Results **41**
4.1 Comparison of fuel systems configurations . . . 41
4.1.1 Power usage . . . 42
4.1.2 Fuel temperature rise . . . 42
4.1.3 Driving energy . . . 42
4.1.4 Cooling capacity . . . 45
4.1.5 Temperature rise due to bypass ratio . . . 45
4.1.6 RM12 modeled LP vs. HP stage temperature rise . . . 47
4.1.7 Throttle valve pressures . . . 47
4.1.8 Electric speed control . . . 48
4.2 Further comparison of fuel system characteristics . . . 48

5 Discussion **51**
5.1 Discussion of results . . . 51
5.1.1 General findings . . . 51
5.1.2 Discrepancies affecting result . . . 52
5.2 Test rig limitations . . . 53

5.3 Gear pump total efficiency curve behavior 53
5.4 Future work 54

6 Conclusion **55**

Bibliography **57**

List of Figures

2.1 RM12 fuel system functional schematic. 6
2.2 MFC bypass control functional schematic. 7
2.3 General example of pump head and efficiency curves. 12
2.4 General example of a system curve. 12
2.5 General evaluation of the system point of operation. 13
2.6 Head vs. flow coefficient for a centrifugal pump [9]. 14
2.7 A Stribeck curve [12]. 15
2.8 A specific diameter vs. specific speed diagram showing different types of pumps [15]. 17
2.9 Gear pump functional sketch [10]. 18
2.10 Gear pump Stribeck-correlated efficiency values. Z is the dynamic viscosity, N is the rotational speed (rad/s) and P is the pump differential pressure [13]. 19
2.11 Cutaway axial swash plate piston pump schematic [12]. 20
2.12 Cutaway schematic layout of a general centrifugal pump [20]. 21
2.13 General pump curves and efficiency curves for centrifugal pumps as a function of specific speed [21]. 22
2.14 Cutaway schematic layout of a partial emission pump [22]. 23

3.1 Extracted kinematic viscocity data for Jet A-1. Derived from [26]. . . 28
3.2 Functional schematic of the test rig. Pressure and flow sensors are omitted from the image. 30
3.3 Visualization of test matrix selection of NH, WFM and WFR, with and without A/B flow. 30
3.4 Normalized outlet pressure correlation. 31
3.5 Estimation of the Joule-Thomson coefficient function using linear regression, expressed as a function of the inlet temperature at the bypass valve. 32
3.6 LP stage pump curves with data points. 33
3.7 HP stage volumetric efficiency. 34
3.8 State estimator code flow chart. 35
3.9 HP stage total efficiency. 36
3.10 Dimensionless centrifugal HP pump curves. 37
3.11 Axial piston pump total efficiency. 38
3.12 Dimensionless electrically driven centrifugal LP stage pump curves. . 39

4.1 Bar plot of the MFP power usage at flight idle. 43

4.2 Bar plot of the MFP power usage at intermediate rated power. 43
4.3 Bar plot of the MFP power usage at maximum A/B thrust. 44
4.4 Bar plot of the fuel temperature rise over the MFP at flight idle. . . . 44
4.5 Bar plot of average MFP driving energy. 45
4.6 Bar plot of cooling capacity. Normalized by System 1. 46
4.7 Scatter plot relating volumetric bypass ratio and temperature rise in System 1. 46
4.8 LP vs. HP stage temperature increase ratio as a function of the volumetric bypass ratio in System 1. 47
4.9 Pressure levels before and after the throttle valve in System 3. 48
4.10 Pump shaft speed vs. volumetric flow delivered to the engine for System 4. 49

List of Tables

4.1 Fuel system numbering description. 41
4.2 Further comparison of fuel system characteristics. 49

1
Introduction

1.1 Background

In any jet engine, a fuel system is needed to supply the engine with metered fuel flow for combustion. However, it may also be utilized to cool other aircraft (A/C) components and systems. In such cases, the fuel itself is used as a heat sink. Depending on the design of the fuel system, fuel properties, and the fuel demand at different engine operating points, the efficiency of the fuel pumps will differ. The energy not imparted as hydraulic work on the fluid will instead largely be introduced as unwanted heat to the fuel system components and the fuel itself. Heating of the fuel in the pumping system degrade the available cooling capacity, thus limiting performance. This issue is exacerbated by an increased necessity to cool electrical components, and a decreased ability of removing heat through the aircraft skin due to an increasing use of composite materials [1]. By improving the performance and efficiency of the fuel pumping system, the cooling ability can be enhanced to better handle increased cooling needs. Furthermore, by reducing the torque power needed to operate the pumps, the impact on engine performance is reduced, improving A/C specific fuel consumption (SFC).

The RM12 engine used in the JAS 39 Gripen C/D fighter jet is developed and maintained by GKN Aerospace Sweden AB. The main fuel pump (MFP) shaft in the RM12 is connected to the high pressure (HP) rotor shaft through a transmission [2]. The rotational speed of the pump shafts are thus proportional to the rotational speed of the HP rotor (NH). Since the NH, and thus the amount of fuel supplied by the MFP is not directly correlated to the engine fuel demand, the MFP is unable to provide the exact amount of fuel needed for all engine operating points. In order to avoid insufficient fuel flow, the pumps are designed to supply a sufficient amount of fuel at some extreme operating condition, for example during maximum thrust or during engine relight at specific points of the flight envelope. As a consequence, the pumping capacity of the MFP is greater than needed for the majority of the engine operating cycle [3]. Hence, the fuel supplied to the combustion chamber must be limited by metering the flow. Depending on the type of pump used, this can be achieved by recirculating excess fuel or by limiting pumping capacity by employing a throttling valve [4, 5]. These methods of restricting the fuel flow impart an irreversible loss of pressure, resulting in heating of the fuel. Alternatively, in order to minimize these irreversibilities, the amount of fuel supplied by the pumps can be set to match the engine requirements. This can be achieved by utilizing pumping

systems that supply fuel flows not directly dependent on the NH, e.g. by using a variable displacement pump or by decoupling the rotational speed of the pump shaft from the jet engine rotational speeds [6].

The variety of solutions for supplying the engine with fuel also implies a variety of advantages and disadvantages. Additional factors important to consider when designing a system include mass, volume, reliability, and cost. An understanding of how all of these factors are affected based on the design is consequently crucial in order to properly review and recommend fuel system designs.

In this thesis, different fuel systems are identified and assessed, using the RM12 engine as a basis. The fuel system model will use inputs from an already created engine performance model operating at different steady state operating points, and return values such as pump power use, efficiencies, and fuel temperature.

In order to improve A/C performance, it is the interest of GKN Aerospace Sweden AB to investigate how the fuel system of the RM12 and possible alternative fuel systems performs at different conditions corresponding to different points of the operating cycle, as it informs future engine development. Specifically, a model of different fuel systems at different operational conditions informs how variations over the operating cycle of the aircraft/engine affect the sizing and design of accessory systems and the accessory gearbox.

1.2 Aim

The task is to model the current fuel system of the RM12 engine operating at steady state conditions, and to identify and model alternative fuel system configurations using publicly available data along with uninstalled system data derived from accessory and engine rig tests at varying operating points.

By comparing the performance of different fuel systems, informative knowledge for the design of future fuel systems is gained. The information gained can be used in future investigations of how A/C thrust, fuel heat sink capability, and SFC is affected.

1.3 Limitations

- The project is carried out over approximately 20 weeks, corresponding to 30 ECTS credits.
- No sensitive data is presented in the final report. Classified information is excluded.
- The inquiry is limited to the fuel pumping system, and since the fuel flow input is entirely based on the requirements for combustion as defined by the engine performance model, the fuel flow needed for cooling of other components is not included in this input. The cooling ability is consequently estimated by the available fuel temperature increase margin after the pumping stages.
- A detailed investigation of the expected lifespan of components in the pumping system will not be conducted, instead the focus is to evaluate the overall performance and reliability.
- A mission is modeled as several steady state operating points, each with a certain time duration. Transient behavior, and by extension the response time of fuel flow changes, is thereby not included.
- The same constant value input pressure is assumed for all steady state operating points, as values affecting the input pressure, such as flight altitude and flight Mach number is classified information.
- The test rig characteristics resemble the currently installed fuel system on the RM12 engine. Unknown data regarding alternative fuel system designs will to a larger extent be based on data from other open sources.
- A fuel system configuration utilizing recirculation of fuel back to the fuel tank will not be considered in order to reduce complexity in possible configurations.
- Pressure losses in the system are handled using system curves. Individual components (such as filters) will not be modeled explicitly.
- Factors such as weight, volume, reliability, and cost will not be included in the model. These factors are instead included as part of the evaluation of different designs.
- The fuel type utilized in the system models is limited to Jet A-1 fuel. No other fuel type will be investigated.

1.4 Specification of the issue being investigated

In order to achieve the goal described in section 1.2, some fundamental questions needs to be answered:

- Which types of pumps and flow rate control methods are relevant for use in the fuel system, and how can they be modeled?
- How much of the energy lost due to pumping inefficiencies and flow restriction contributes to heating of the fuel and pump system components respectively, and what are the sources of these inefficiencies?
- How can a fuel system be modeled to obtain the sought after knowledge (such as efficiencies, and pumping power), for any given steady state operating point?
- In which aspects are different fuel system configurations preferable?

2
Theory

2.1 Fuel system overview

The main purpose of a jet engine fuel system is to supply the engine core with a metered fuel flow for combustion at sufficient pressures in order to generate thrust. Additionally, it may be tasked with supplying pressurized fuel for afterburner (A/B) combustion. Furthermore, the fuel system may be required to supply fuel flow for use as coolant, or to supply pressurized fuel that can be utilized as hydraulic fluid for use in engine actuation. Actuation may include movement of stator vane angles or geometry change in the engine outlet nozzle. More specifically, the RM12 fuel system is used to supply both main and A/B combustion, to supply coolant flow, and to supply pressurized hydraulic fluid used to move stator vane angles in the engine compressor and fan.

The fuel system in the RM12 consists of multiple components. A basic functional schematic of the system is shown in Fig. 2.1. The dotted line designate components included in the MFP and denotes parts of the fuel system that are considered in this thesis. The purpose and function of the components shown in Fig. 2.1 are described below.

2.1.1 Aircraft booster pump

The objective of the booster pump is to transfer fuel from the airframe fuel tank to the LP pump at all operating conditions. This includes a pressure buildup, helping the LP pump operate above the required net positive suction head ($NPSH_r$). While the booster pump plays a crucial role in transferring fuel from the fuel collector tank to the MFP, investigations regarding the booster pump and its performance are beyond the scope of this study.

2.1.2 Main fuel pump

The MFP consists of multiple components, integrated in the same housing assembly. The purpose of the MFP is to supply pressurized flow to the main engine core, and to pressurize fuel for the A/B before it enters the A/B pump (ABP) and A/B fuel controller (ABC). Additionally, it provides pressurized servo fuel flow.

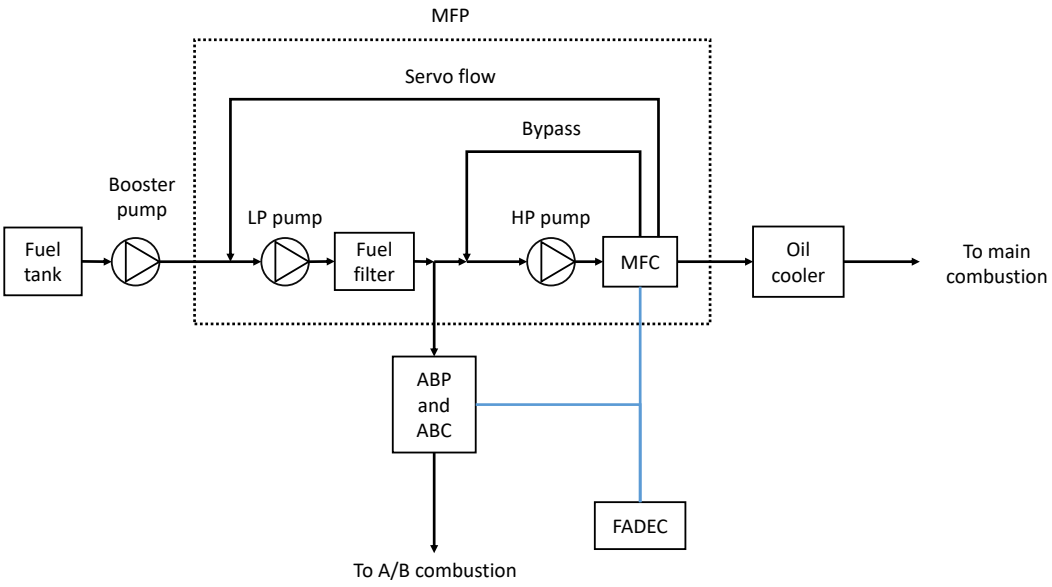

Figure 2.1: RM12 fuel system functional schematic.

2.1.2.1 Pumping stages and fuel filter

The MFP contains two pumping stages, a LP pump, and a HP pump. The LP stage is needed to force the fuel through the filter and to ensure cavitation is not present in the HP stage. The HP stage is necessary to achieve the high pressure head needed by the engine during operation. The LP pump consists of a centrifugal impeller with an axial inducer. The inducer allows the LP pumping stage to operate at lower $NPSH_r$, allowing for operation without cavitation for a wider set of operating conditions. The LP pump serves as an initial pumping stage for both the ABP and HP pump.

The HP pump consists of a positive displacement gear pump contributing the greater part of the fuel pressurization. The LP and HP pumps both share the same drive shaft. The pump drive shaft is driven by the accessory gearbox (AGB), which in turn is powered by a bevel gear to the engine HP rotor shaft. The rotational speed of the pumping stages are thus proportional to the rotational speed of the engine HP rotor.

A fuel filter is placed in between the LP and HP pumps. The purpose of this filter is to remove contaminants in the fuel before it enters sensitive components downsteam in the fuel system. The filter location downstream of the LP pumping stage is made possible as the centrifugal pump used in this stage is insensitive to contaminants.

2.1.2.2 Main fuel control, bypass and servo flow

The main fuel control (MFC) is a hydromechanical control system that, based on inputs from the FADEC, meters the fuel for the engine main combustion by recir-

culating excess fuel back to the HP pump inlet through a bypass channel, as seen in Fig. 2.2. For further information on the FADEC, see Sec. 2.1.5. By controlling the opening area of a bypass valve based on the pressure differential over a metering valve, the pressure differential over the metering valve can be set constant. With a constant pressure differential over the metering valve, the volume flow to the engine can be precisely controlled by changing the nozzle area of the metering valve. This concept can be explained by Eqn. 2.1, which is derived from the Bernoulli equation.

$$Q = C_d A_2 \sqrt{\frac{2(p_1 - p_2)}{\rho\left(1 - \left(\frac{A_2}{A_1}\right)^2\right)}} \tag{2.1}$$

where the discharge coefficient C_d is used to account for the valve geometry. The discharge coefficient is dependent on the area ratio between valve inlet and outlet as well as the Reynolds number. Q is the volume flow through the area change. p is the fluid pressure, ρ is the density of the fluid, and A is the orifice area. Notations 1 and 2 represent valve inlet and outlet respectively.

Value changes of the discharge coefficient tend to be quite small despite large changes in valve area ratio or Reynolds number, assuming the Reynolds number is sufficiently high [7].

The flow not needed for combustion passes through the bypass valve, where the flow experiences a pressure drop and is recirculated back to the HP pump inlet. A functional schematic of the MFC bypass control can be seen in Fig. 2.2.

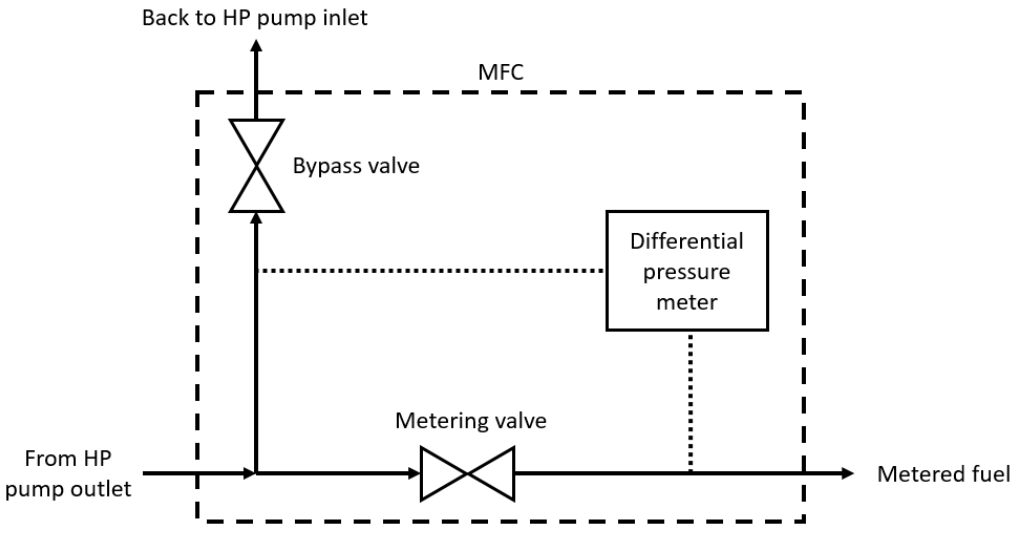

Figure 2.2: MFC bypass control functional schematic.

The MFC also control the servo flow. This flow supplies hydraulic actuation fluid to movable systems and internal servo systems in the MFC. During steady state operation, actuation is typically not needed, however a certain leakage flow is to be expected and must be taken into account. The servo flow is diverted from the high

pressure flow after the HP pump, used, and returned upstream the LP pump.

2.1.3 A/B fuel pump and A/B fuel control

The A/B fuel pump (ABP) is used to pressurize fuel further before it enters the A/B. A centrifugal, vapor core-controlled pump is used. The amount of pressurized fuel is controlled by the hydromechanical A/B fuel controller (ABC).

2.1.4 Oil cooler

The oil cooler is placed after the HP pump and MFC. The oil cooler uses fuel as a heat sink in order to cool oil used in different parts of the engine system. The temperature of the fuel therefore have an impact on the cooling performance. By decreasing the fuel temperature for a given engine operational condition, the amount of cooling available is increased. Note that the fuel temperature also have to stay below a certain threshold in order to prevent coking. This constitutes an upper fuel temperature limit, which depends on the type of fuel used [3].

2.1.5 Full authority digital engine control

The full authority digital engine control (FADEC) is the brain of the engine. The FADEC receives various inputs, from both the pilot and the engine and calculates the proper subsystem control outputs. In Fig. 2.1, the communication between the FADEC and MFC/ABC is marked with blue lines.

2.2 Pump and system curves

The use of pump and system curves is a common way of visualizing pump and system performance, typically as a function of pump/system head versus flow and pump efficiency versus flow. These terms are defined in the sections below, followed by a short explanation of pump and system curve plots.

2.2.1 Definition of head

Consider a one-dimensional steady flow through a pump with an incompressible fluid. Let station 1 and 2 denote the inlet and outlet respectively. Applying the steady flow energy equation, the total energy imparted to the fluid can be expressed as the following:

$$\dot{Q} + \dot{W}_s + \dot{W}_v = -\dot{m}(u_1 + \frac{p_1}{\rho} + \frac{1}{2}V_1^2 + gz_1) + \dot{m}(u_2 + \frac{p_2}{\rho} + \frac{1}{2}V_2^2 + gz_2) \qquad (2.2)$$

where $\dot{Q}$ is the heat power added to the fluid, $\dot{W}_s$ is the added shaft power, $\dot{W}_v$ is the added viscous power, $\dot{m}$ is the mass flow, u is the internal energy, V is the mean flow velocity, and z a height relative some point.

Since the flow is incompressible, $\dot{m}$ can be removed. Furthermore, by assuming adiabatic flow and static walls (thus no viscous work), Eqn. 2.2 can be transformed into the following:

$$w_s = -\Big(u_1 + \frac{p_1}{\rho} + \frac{1}{2}V_1^2 + gz_1\Big) + u_2 + \frac{p_2}{\rho} + \frac{1}{2}V_2^2 + gz_2 \tag{2.3}$$

Where w_s is the shaft work transferred to the fluid per unit mass. By dividing Eqn. 2.3 by the gravitational constant g each term can be expressed as a length, and by rearranging the equations, we get the following:

$$\frac{w_s}{g} = \frac{p_2}{\rho g} + \frac{1}{2g}V_2^2 + z_2 - \Big(\frac{p_1}{\rho g} + \frac{1}{2g}V_1^2 + z_1\Big) + \frac{u_2 - u_1}{g} \tag{2.4}$$

or

$$\frac{w_s}{g} = \Delta H + \frac{u_2 - u_1}{g} \tag{2.5}$$

where

$$H = \frac{p}{\rho g} + \frac{1}{2g}V^2 + z \tag{2.6}$$

ΔH is refered to as the total dynamic head, as it contains pressure, velocity and elevation head terms. The total dynamic head is a common measurement for the useful energy imparted to a fluid by a pump, and can be interpreted as the height difference that can be generated by a pump if the pressure and velocity head is transformed into potential energy without losses. Note that ΔH is not the only term on the right hand side of Eqn. 2.5. The second term represent the increase in specific energy due to the shaft work on the left hand side, and thus represent pumping losses added as heat to the fluid [8]. This is important when defining efficiency, which is covered in Sec. 2.2.2.

It is also important to note that the height difference between the inlet and outlet of the pumps covered in this thesis are negligible. It can also be assumed that the velocity is similar at the inlet and outlet of the pump. Combined with the high expected pressure differential, ΔH can safely be approximated as $\Delta p/(\rho g)$. These assumptions are commonly made with regards to pumps [9].

2.2.2 Pump efficiency

In order to quantify pump efficiency Eqn. 2.5 is revisited. Recall that the equation show the head form of the energy equation, where the left hand side represent the shaft work added to the fluid by the pump. The right hand side of the equation

contain ΔH, which represent the useful energy added to the fluid, and $\Delta u/g$ represent the part of the shaft work that instead increase the internal energy of the fluid, expressed as a fluid temperature rise. By defining the total efficiency, η, as useful work, divided by the total added shaft work using the terms in Eqn. 2.5, the following can be shown:

$$\eta = \frac{\text{Useful work}}{\text{Added work}} = \frac{\Delta Hg}{w_s} = \frac{\Delta Hg\dot{m}}{\dot{W}_s} = \frac{\Delta Hg\rho Q}{\dot{W}_s} \tag{2.7}$$

By approximating the total dynamic head using the pressure differential and density as described in Sec. 2.2.1, Eqn. 2.7 can be rewritten as the following:

$$\eta = \frac{\Delta pQ}{\dot{W}_s} \tag{2.8}$$

If the added work is instead expressed as the sum of useful work and the increase in internal energy of the fluid, assuming that the increase in internal energy results in a temperature rise ΔT, η can instead equivalently be expressed as:

$$\eta = \frac{\Delta Hg}{\Delta Hg + \Delta u} = \left(1 + \frac{\Delta u}{\Delta Hg}\right)^{-1} = \left(1 + \frac{c_p \Delta T}{\Delta Hg}\right)^{-1} \tag{2.9}$$

Note that Eqn. 2.9 can be evaluated without knowing the mass flow. The total pump efficiency can also be expressed as the product of other component efficiencies. An understanding of how component efficiencies behave, and thereby how they affect the total efficiency of a pump may be important when, for example, the efficiency performance of a hypothetical pump is modeled. It is common to divide the total pump efficiency as the product between the volumetric efficiency η_v and the mechanical efficiency η_m [10].

The volumetric efficiency is defined as the actual flow rate delivered by the pump over the ideal theoretical flow rate (see Eqn. 2.11). The actual flow rate may be lower than the theoretical ideal flow rate through a pump due to leakage flows, in essence fluid recirculated within the pump.

$$Q = Q_{\text{ideal}} - Q_{\text{leakage}} \tag{2.10}$$

$$\eta_v = \frac{Q}{Q_{\text{ideal}}} = \frac{Q_{\text{ideal}} - Q_{\text{leakage}}}{Q_{\text{ideal}}} \tag{2.11}$$

In a positive displacement pump, the volumetric efficiency can be expressed as ideal displacement per pump shaft unit of rotation, divided by the actual displacement per unit of rotation. The ideal displacement is usually easily defined given a known pump geometry.

$$\eta_v = \frac{Q}{Q_{\text{ideal}}} = \frac{V_d \omega}{V_{d,\text{ideal}} \omega} = \frac{V_d}{V_{d,\text{ideal}}} \tag{2.12}$$

where ω is the rotational speed of the pump shaft.

The mechanical efficiency is defined as the ideal useful work divided by the actual shaft work required to drive the pump as can be seen in Eqn. 2.13:

$$\eta_m = \frac{\Delta H g \rho Q_{\text{ideal}}}{\dot{W}_s} \tag{2.13}$$

Thus multiplying Eqn. 2.11 and 2.13 returns Eqn. 2.7:

$$\eta = \eta_v \eta_m = \frac{Q}{Q_{\text{ideal}}} \frac{\Delta H g \rho Q_{\text{ideal}}}{\dot{W}_s} = \frac{\Delta H g \rho Q}{\dot{W}_s} \tag{2.14}$$

Note that the division of the total efficiency into volumetric and mechanical components is not the only possible way of dividing the total efficiency, and that other formulations can be used.

The impact of different pump control methods on the total system efficiency is covered in Sec. 2.5.

2.2.3 Pump curves

A pump curve typically correlate the volume flow through the pump with some type of quantity, typically ΔH, pump efficiency or pump power. Pump curves are typically supplied by pump manufacturers or suppliers, and the exact shape of these curves vary greatly depending on pump model and type. The expected pump curve shapes are covered for different pump types in Sec. 2.4.2. Sometimes multiple curves of the same type are shown in the same figure, denoting different pump speeds or impeller diameters. A general, purely illustrative, example is shown in Fig. 2.3. The best efficiency point (BEP) is commonly used to denote the flow where the maximum pump efficiency is located.

Also note that pumps can be connected in either parallel or in series. When pumps are connected in series, the volume flow is unaffected (assuming identical pumps), however the collective pump head becomes the addition of each individual pump head. Thus, a new pump curve for the series connected pumps can be estimated by simply adding the head value of the individual pump curves at every point.

2.2.4 System curve

A system curve typically show the head resistance at a point of the system as a function of the volume flow through the system. A general example can be seen in Fig. 2.4. The head shown at zero flow represent the static resistance, or the resistance that needs to be overcome in order to generate any flow through the system, this could for example be caused by a height difference or a resistive pressure difference present in the system. The additional resistance generated beyond the point of zero flow is called the dynamic resistance, and is typically proportional to the square of the flow. The curve can be made steeper by increasing the resistance in the system.

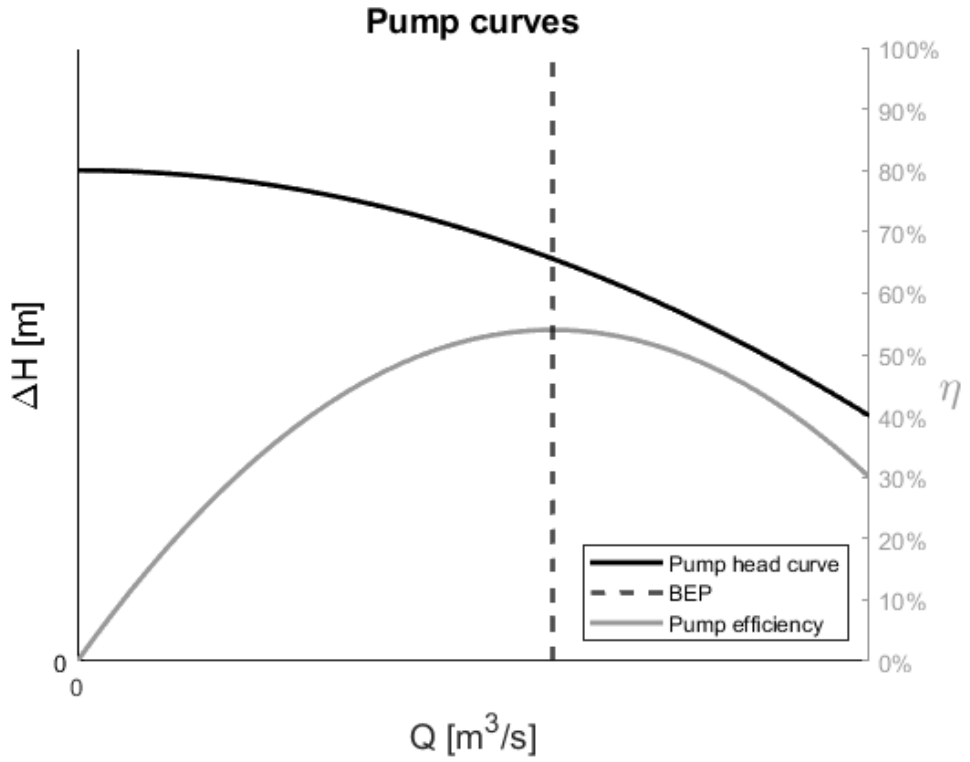

Figure 2.3: General example of pump head and efficiency curves.

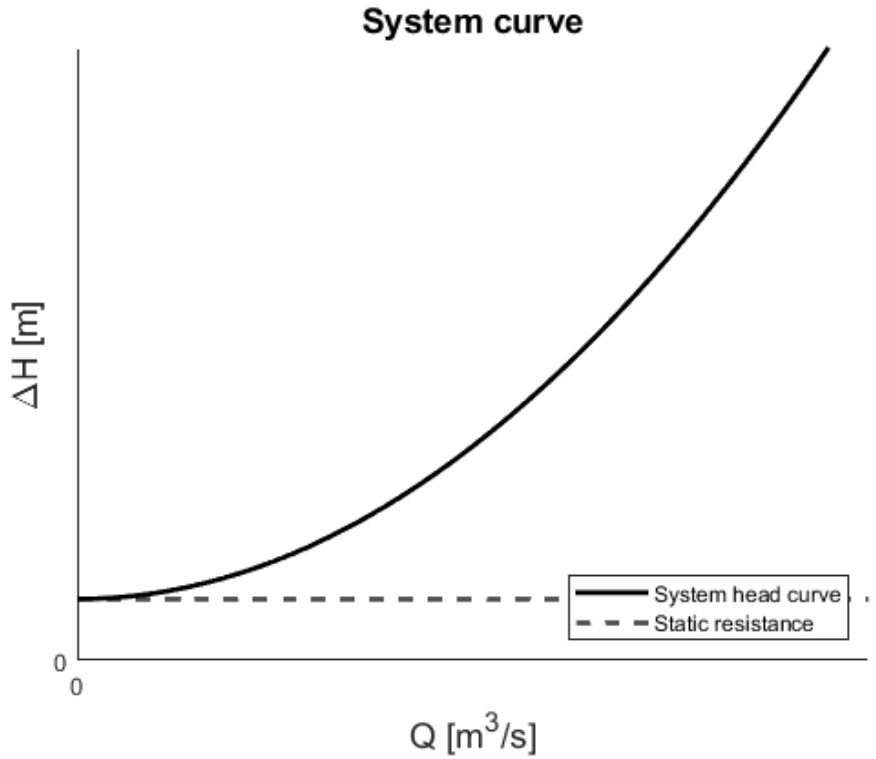

Figure 2.4: General example of a system curve.

2.2.5 System performance

Pump and system curves can be combined in order to estimate at which conditions a pumping system operates. When combined, the pump head curve represents the available head at a certain flow, whereas the system head represents the required head for a certain flow. The actual operational point of a system operating at steady state is therefore located at the intersection between the pump and system head curves. This concept is demonstrated in Fig. 2.5. Note that the pump efficiency is lower at the point of operation, as compared to the BEP in the example.

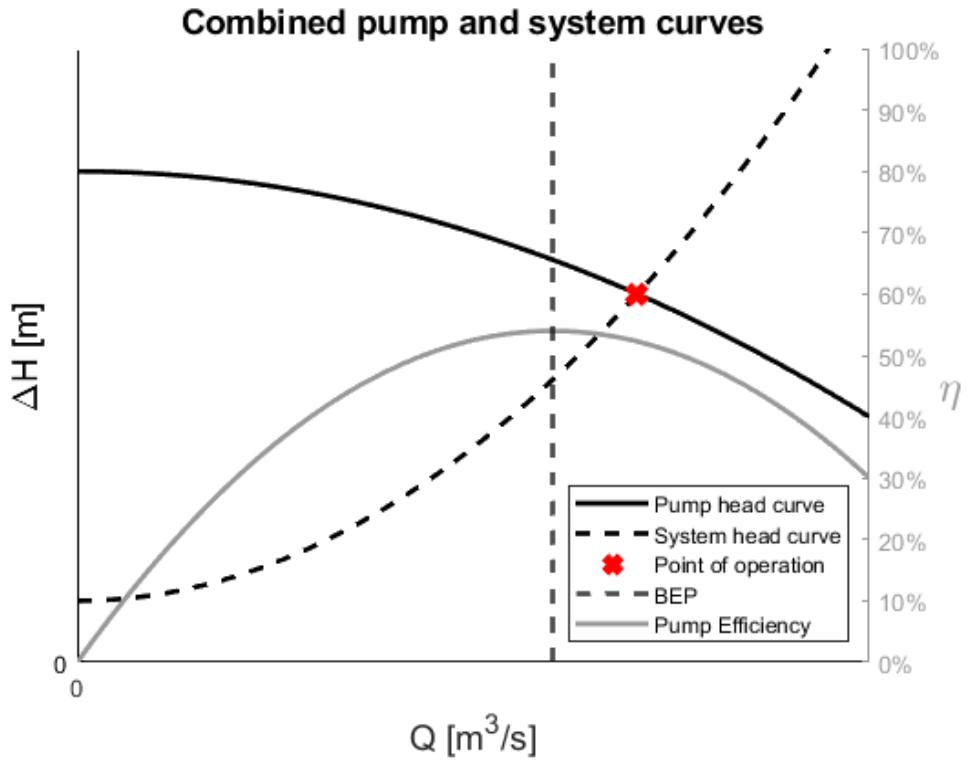

Figure 2.5: General evaluation of the system point of operation.

2.3 Dimensionless performance parameters

Dimensionless performance parameters, derived through dimensional analysis are commonly used in order to get a comprehensive understanding of the general behavior of a pump. Furthermore, dimensionless performance parameter data may be used in order to predict pump performance at different scales or speeds given limited empirical data. They may also be used in pump selection schemes [9].

2.3.1 Head and flow coefficients

The flow coefficient is defined as:

$$\phi = \frac{Q}{\omega D^3} \tag{2.15}$$

and the head coefficient is defined as:

$$\psi = \frac{g\Delta H}{(\omega D)^2} \tag{2.16}$$

where ω is the rotational speed of the pump, and D is the pump characteristic diameter.

The head coefficient ψ can be assumed to only depend on the flow coefficient ϕ given the assumption that pump surface finish is of small importance, and a sufficiently large Reynolds number [9].

The dimensionless head and flow coefficients may be used to collapse pump curve data for several pump diameters and speeds into a single curve, given dynamic similarity. Thus, if dynamic similarity can be assumed, pump performance at different conditions can be assessed using a single curve. Furthermore, if dynamic similarity holds true, all dimensionless parameters including efficiency are identical [9]. In Fig. 2.6, the dimensionless head and flow coefficients are plotted for a centrifugal pump at different speeds. Note that dynamic similarity does not hold true when cavitation is present.

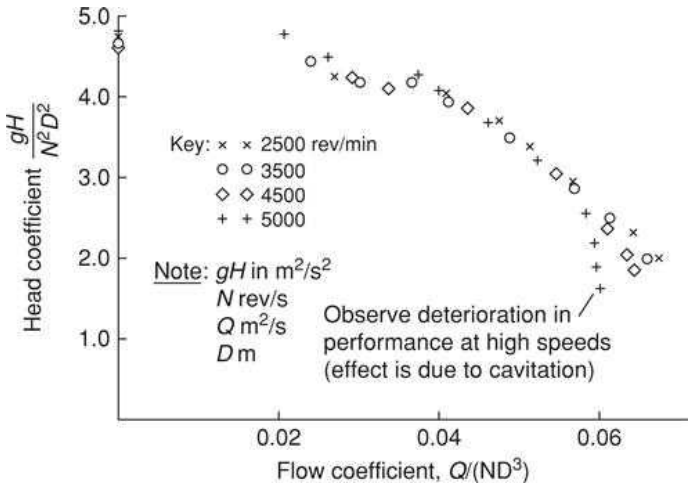

Figure 2.6: Head vs. flow coefficient for a centrifugal pump [9].

2.3.2 Specific speed and specific diameter

Specific speed and specific diameter are commonly used together as a means of assessing which type of pump is appropriate for a given duty, knowing some performance parameters. The specific speed is defined as [9, 11]:

$$\omega_s = \frac{\phi^{1/2}}{\psi^{3/4}} = \frac{\omega\sqrt{Q}}{(g\Delta H)^{3/4}} \tag{2.17}$$

The definition shown in Eqn. 2.17 is truly dimensionless and defined in SI units. Note that several other varieties exist, commonly excluding the gravitational constant g, and using non-SI units. Careful inspection of the version used is needed when comparing empirical data.

The specific diameter is defined as [9, 11]:

$$d_s = \frac{\psi^{1/4}}{\phi^{1/2}} = \frac{(D\Delta Hg)^{1/4}}{\sqrt{Q}} \tag{2.18}$$

Similar to the specific speed, Eqn. 2.18 is truly dimensionless and uses SI units. The specific diameter may also take on several forms.

2.3.3 Stribeck curve correlations for positive displacement pumps

To the authors' knowledge there is no way of accurately predicting the efficiency characteristics given a positive displacement pump without some applicable empirical data, derived from either CFD or experiments. One possible way of approximating the efficiency behavior of certain types of positive displacement pumps is derived from the study of tribology by the use of the Stribeck curve. The Stribeck curve is a general description of how the coefficient of friction between two lubricated surfaces is altered depending on the relative velocity of the two surfaces, the dynamic viscosity of the fluid and the applied normal load [12]. In Fig. 2.7, the Stribeck curve is shown, where μ_f is the coefficient of friction between two sliding surfaces, U is the relative sliding velocity and W is the applied normal load per unit width. n_1 and n_2 mark the approximate boundaries of different boundary lubrication regimes.

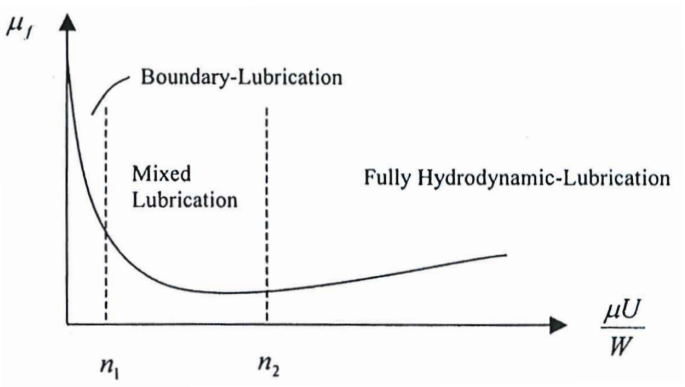

Figure 2.7: A Stribeck curve [12].

By assuming that the efficiencies in the pump are largely dependent on the lubrication conditions within the machine, and that the sliding velocity and applied normal force can be substituted by the pump rotational speed and pressure differential respectively, the dimensionless Stribeck number (also known as the dimensionless viscosity), is formed. The Stribeck number is defined as [13]:

$$\text{Stribeck number} = \frac{\mu\omega}{\Delta p} \tag{2.19}$$

where μ is the dynamic viscosity and Δp is the pump static pressure increase.

By relating empirical efficiency data with the Stribeck number, it may be possible to estimate an approximate general efficiency behavior of different types of positive displacement machines, without designing and simulating a detailed pump. Previous papers modelling efficiency of positive displacement machines utilizing the Stribeck curve include [13], in which component efficiencies are correlated to the Stribeck number for multiple gear pumps at differing operational conditions. In [12], a tribological approach is used to formulate a model of the mechanical efficiency of axial piston pumps. The model contains coefficients which need to be evaluated using empirical data. It is stressed that the model itself is not specifically applicable to any one type of displacement pump, but can be used for different types of positive displacement types given appropriate empirical data. In [14], the efficiency characteristics of an axial piston motor is described by correlating experimental data to the Stribeck number for different fluid viscosities.

2.4 Pump type theory

This section covers the theory regarding pump type selection and general descriptions of relevant pump types for use in a jet engine main fuel system covered in this thesis.

2.4.1 Specific diameter vs. specific speed diagrams

One way to assess the feasibility of different pump types is through the use of specific diameter versus specific speed diagrams. These diagrams contain contour plots denoting expected regions suitable for different types of pumps, and their expected operational efficiency. These diagrams may thus be used to get a general understanding of which types of pumps that are feasible for a certain application. Fig. 2.8 show efficiency contour plots for several types of hydraulic pumps.

Note that several other factors that cannot be included in a specific diameter versus specific speed diagram may affect the choice of pump type. This may include absolute limitations on flow and head delivered by the pump, cost, weight, size, reliability and so on. These factors are important to include in any consideration regarding pump selection.

2.4.2 Pump type descriptions

Descriptions of different pump types used in this thesis, along with explanations for their selection as applicable fuel system pumps is covered in the sections below.

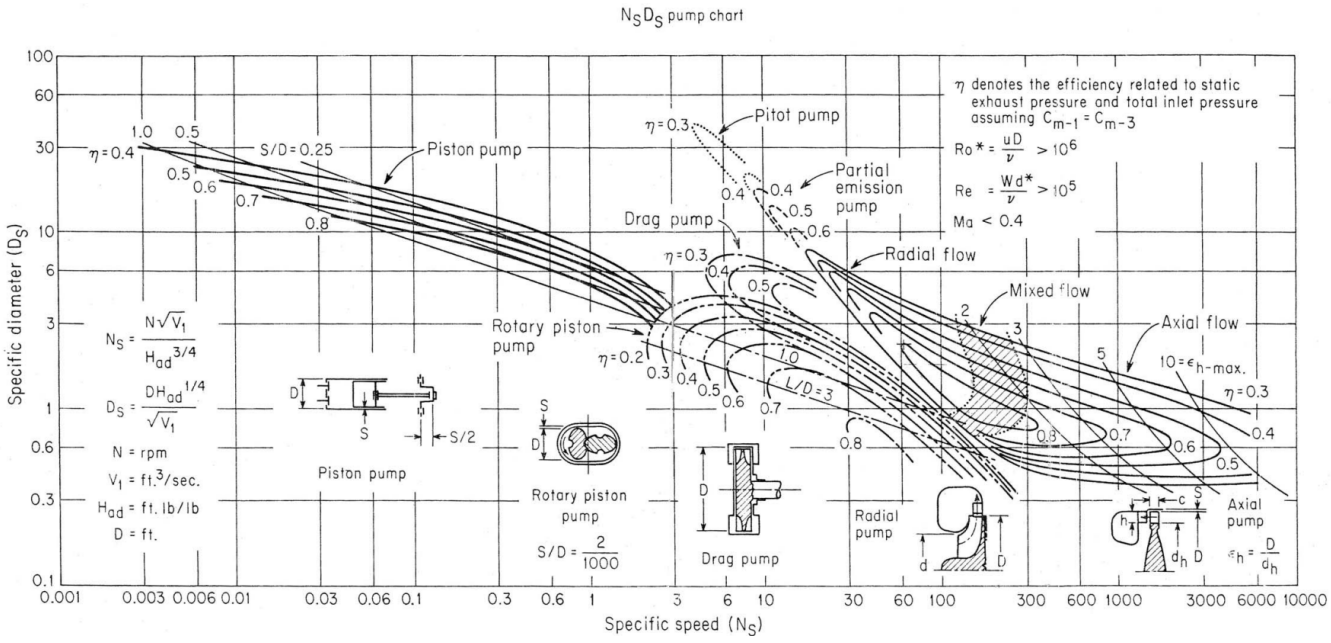

Figure 2.8: A specific diameter vs. specific speed diagram showing different types of pumps [15].

2.4.2.1 Pump type classifications

The pumps covered in this thesis can be placed into one of two categories; hydrostatic positive displacement pumps or hydrodynamic centrifugal pumps. Positive displacement pumps impart a discrete pressure increase to the fluid by displacing a fluid enclosed in a fixed volume. By forcing a flow relative to some system resistance, the pressure of the fluid increases. The flow rate of a positive displacement pump is therefore largely dependent on the volume of fluid that can be displaced per unit of time [8]. Centrifugal pumps on the other hand continuously increase the energy of the fluid through the use of a rotating impeller, which is subsequently transformed into a pressure. The amount of flow that the pump is able to generate is thus dependent on the pressure differential over the pump, and vice versa, as the amount of energy that the impeller is able to impart on a given volume of fluid is dependent on the flow rate through the pump [16].

The tolerances in positive displacement pumps are typically small, in order to minimize internal leakage of trapped fuel. However, some leakage is typically needed in order lubricate sliding surfaces and thus limit wear. These small tolerances make positive displacement type pumps vulnerable to vapor and contaminants in the fluid, which typically does not affect centrifugal pumps to the same extent [3, 8]. Positive displacement pumps can supply useful pressure at both low and high rotational speeds, and have the ability to reprime from completely dry conditions [8]. Centrifugal pumps are typically better suited than positive displacement pumps for operation at high rotational speeds [17].

2.4.2.2 External gear pump

The external gear pump, is a type of positive displacement pump which impart a displacement on a fluid by entrapping it in the voids between rotating gear teeth and the pump casing. As the gear teeth interlock, the entrapped fluid is forced to eject at the outlet. This causes the pressure to rise at the outlet to meet the system resistance for the imparted flow. A gear pump typically consists of two gears, a driving gear driven by the pump's input shaft, and a driven gear [8]. The main types of internal leakage in a gear pump consist of the radial leakage and axial leakage. The radial leakage consists of fluid passing over the gear teeth ridges, whereas the axial leakage consist of fluid escaping back to the inlet at the contact surface of the gear wheel sides and pump side plates. Fig. 2.9 show the operational principle of the gear pump, as well as the main types of internal leakage expected in a gear pump.

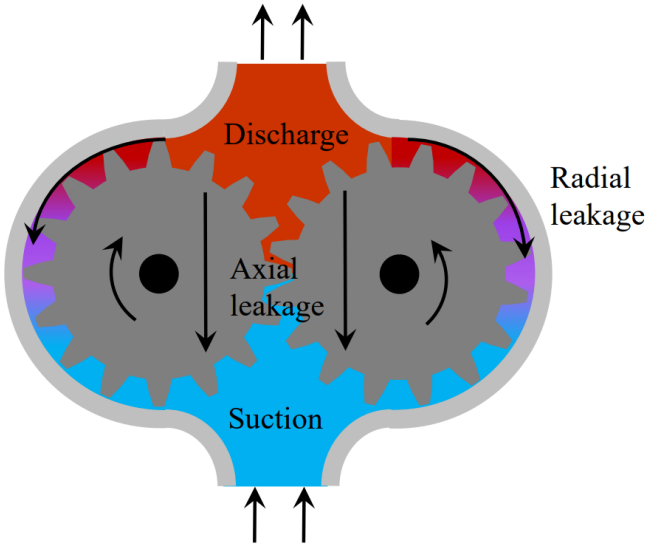

Figure 2.9: Gear pump functional sketch [10].

Gear pumps have long been favored for use in the HP stage of jet engine fuel systems. This is due to its ability of supplying sufficiently pressurized fuel at low as well as high rotational speeds. Another reason for the widespread adoption of gear pumps is due to their simple design and benign failure modes, and thus safe operational characteristics. As the pump is worn, the leakages in the pump increase in a predictable manner, over time degrading in capacity without any sudden failures [8]. An external gear pump is also used in the RM12 engine fuel system HP stage.

As the external gear pump is a positive displacement machine, the amount of pressurized fluid supplied by the pump is largely dependent on the rotational speed of the pump, with some variations due to leakage flows, which is affected by the pressure differential and rotational speed of the pump. The gear pump head curve can thus be idealized as an essentially straight line, with only minor variations in flow with larger pressure variations, for a certain rotational speed. The efficiency characteristics of gear pumps can typically be related to the Stribeck number, as

mentioned in Sec. 2.3.3. Fig. 2.10 is used here to illustrate how the gear pump component efficiency curves typically behave and what efficiencies to expect.

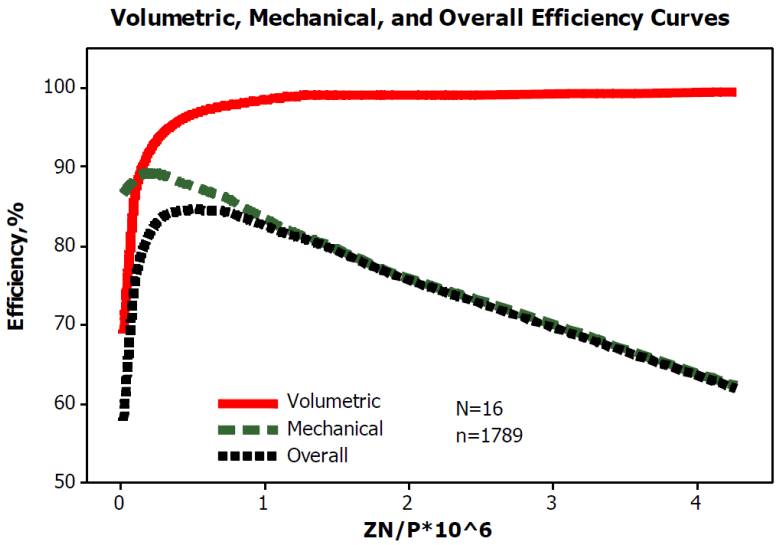

Figure 2.10: Gear pump Stribeck-correlated efficiency values. Z is the dynamic viscosity, N is the rotational speed (rad/s) and P is the pump differential pressure [13].

However, as the efficiency correlations above all have been derived using hydraulic oil as the pump fluid medium, the actual operation using jet fuel may prove substantially different. In [18], the tribological conditions of a gear pump using jet fuel is modeled. It is found that the low viscosity of the fuel in combination with tight tolerances needed to ensure good volumetric efficiency give rise to exceedingly thin lubricating film layers at the submicrometer level. For this reason, the surface roughness of the contact surfaces may impact the behavior of the pump. Furthermore, in [17] it is stated that a high rotational speed may negatively impact the mechanical efficiency and thereby the total efficiency due to increased fluid and mechanical friction.

2.4.2.3 Axial swash plate piston pump

The axial swash plate piston pump is a variable displacement pump. The pump contain pistons oriented in parallel and placed axisymmetrically around the pump shaft axis. The piston cylinders are located in an axially rotating cylinder block connected to the pump shaft. A piston reciprocates back and forth in each cylinder, drawing in and expunging liquid once every full rotation. The pump cylinder block is pushed against a stationary valve plate containing elongated port openings for the inlet and outlet. The back end of the cylinders are allowed to slide against an angled stationary swash plate controlling the reciprocating motion of the pistons. By altering the swash plate angle α, the piston stroke length can be altered. This allows for adjustment of the volume of displaced fluid relative the pump shaft ro-

tation. The amount of displaced fluid per unit time is thus dependent on both the rotational speed of the shaft, as well as the swash plate angle α. The entire pump is typically placed in a fluid-filled pump housing. Most commonly, the pump utilize nine or seven pistons. An odd number is used in order to reduce the amplitude of flow ripples [19]. A typical axial swash plate piston pump is shown in Fig. 2.11.

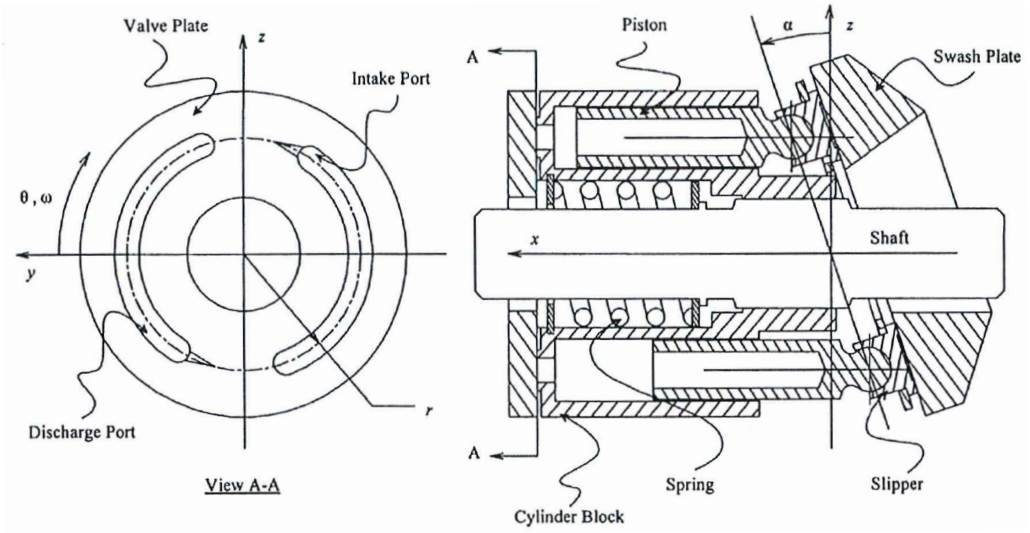

Figure 2.11: Cutaway axial swash plate piston pump schematic [12].

Axial piston pumps are able to supply high pressures while operating at high efficiencies compared to other displacement pumps. It is the most commonly used pump type in aircraft hydraulic control systems, however the mechanical complexity limits reliability in comparison to the other pump alternatives listed [19].

The axial piston pump has been utilized as a main fuel pump, but only to a limited extent, according to [3] and [8]. Furthermore, the authors' of this thesis have come across information stating that at least one version of the RM6 engine used in the Saab 35 Draken fighter jet employed a dual variable axial piston pump MFP configuration with a stated total efficiency of approximately 80% at maximum flow and pressure. The dual configuration was most likely used to ensure safe operation despite the high mechanical complexity and relatively low reliability of each pump.

A variable axial piston pump was used to model a variable flow fuel system in [1]. Since the axial piston pump is a positive displacement machine, the pump head and efficiency curve behavior is similar to the previously discussed external gear pump.

2.4.2.4 Radial centrifugal pump

The radial centrifugal pump is a hydrodynamic type pump with a mean outflow direction parallel to the radial plane relative the pump shaft axis. This type of pump is used in the LP stage of the RM12 pumping system, paired with an inducer. The

radial centrifugal pump has the lowest specific speed of all the common centrifugal pump types, as can be seen in Fig. 2.8. The centrifugal pump imparts kinetic energy to the flow by means of an impeller. The flow is collected into a volute at the impeller periphery. The kinetic energy is subsequently transformed into a pressure increase. Fig. 2.12 show the basic layout of a centrifugal pump.

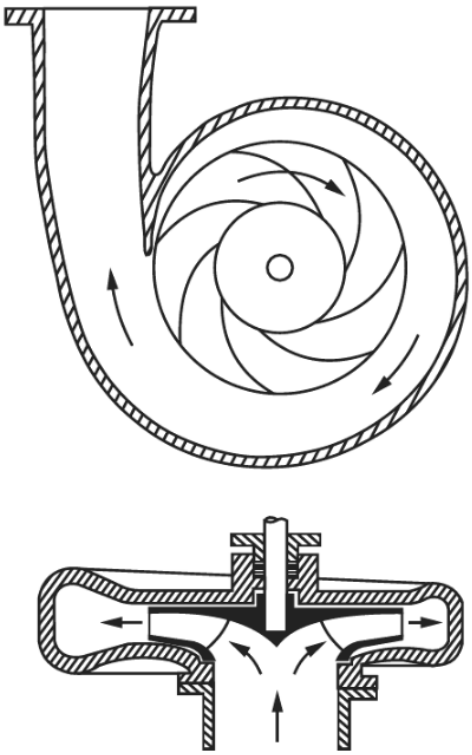

Figure 2.12: Cutaway schematic layout of a general centrifugal pump [20].

The basic shapes of the pump head and efficiency curve for general centrifugal pumps is shown in Fig. 2.13 as a function of specific speed. Note that η_{opt}, H_{opt} represent the efficiency and head BEP, respectively. q^* express the volumetric flow rate through the pump, normalized for the flow at the BEP. The specific speed n_q is defined using rotational speed in RPM, volume flow in cubic meters per second and head in meters, omitting the gravitational constant g.

A centrifugal pump typically requires a separate positive displacement pump for priming the system at engine start up because of the poor head build up at low speeds. It may be possible for a centrifugal pump to have self priming capabilities in a variable speed system granted it can be spun at high speed [3].

2.4.2.5 Partial emission pump

The partial emission pump, also referred to as a forced vortex pump, Barske pump, tangent pump, or Sundyne pump, is a type of low specific speed centrifugal pump.

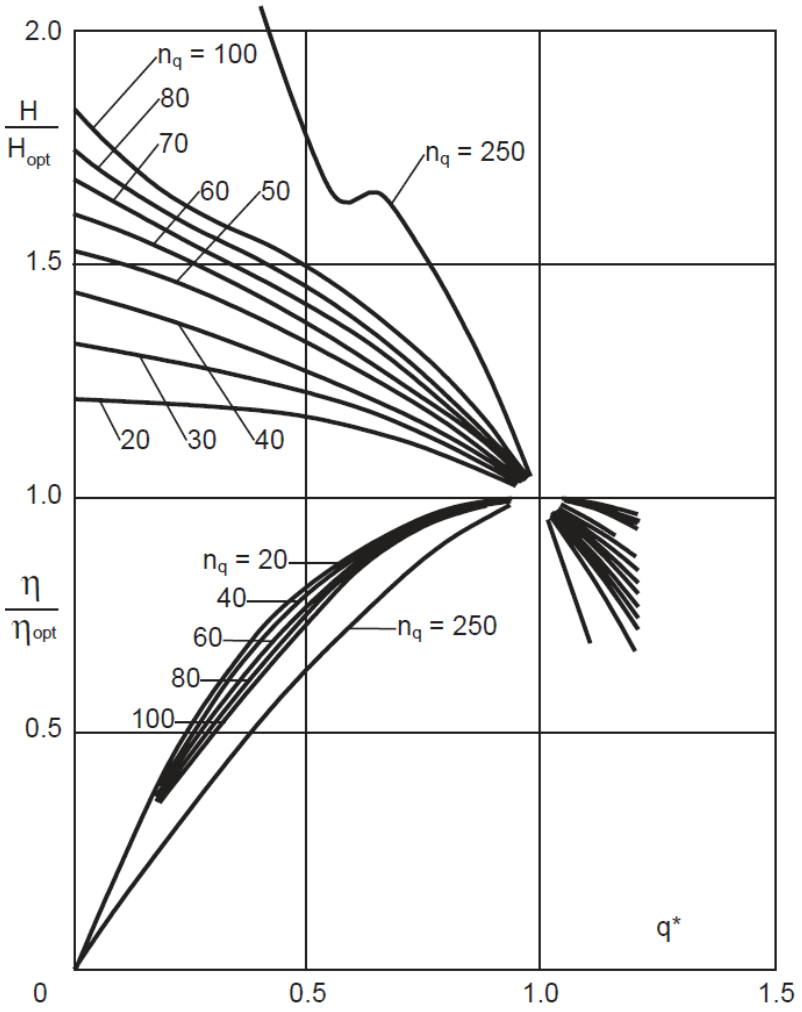

Figure 2.13: General pump curves and efficiency curves for centrifugal pumps as a function of specific speed [21].

Partial emission pumps are typically comprised of straight impeller blades enclosed in a constant cross section housing, using one or more conical diffusers, which allow for a simple and compact design. The straight radial blades are not subjected to any considerable bending stress by the high centrifugal forces that are present. Additional advantageous design features of a partial emission pump include that there is no need for any wear rings or labyrinth seals and the large clearances between blades and housing decrease required manufacturing tolerances and thus reduce manufacturing cost [17, 23]. A visual representation of a partial emission pump can be seen in Fig. 2.14. This pump design allows for high rotational speed and is capable of delivering high head and small flow rates. The pump can thus be made to minimize size and weight.

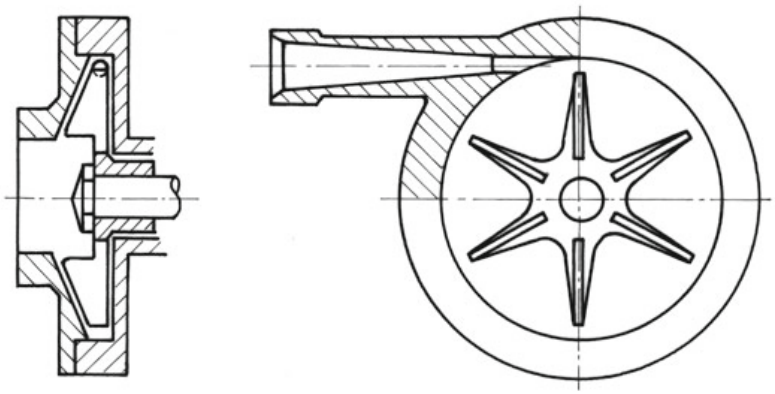

Figure 2.14: Cutaway schematic layout of a partial emission pump [22].

The pump curve of a partial emission pump is exceedingly flat with a sharp drop-off close to the maximum flow rate [24]. Partial emission pumps operate at higher efficiencies at lower specific speeds compared to conventional radial centrifugal pumps, as can be observed in Fig. 2.8.

2.5 Flow rate control methods

Fuel pumps in A/C are typically sized based on three operating points; the ground engine starting condition, in-flight windmill relight, and the worst-case conditions for maximum thrust at sea level during takeoff [3]. This implies that the pump will provide more fuel than the engine requires during other points of operation if the flow is not limited.

This section describes methods that may be employed to control the amount of flow delivered to the engine by a fuel pumping system.

2.5.1 Flow control by recirculation

Recirculation is a common way of limiting the amount of flow delivered to the combustion chamber by a pump. As the flow delivered by the pump is dependent on the rotational speed of the pump shaft, the excess fuel can be recirculated back to the pump inlet, or alternatively back to the fuel tank. The RM12 fuel system uses this method to limit the fuel delivered by the HP pump by recirculating excess fuel back to the HP pump inlet, as mentioned in Sec. 2.1.2.2. While this method offers a simple solution, it adversely affects the temperature increase, as the same fluid may be passed through the pump several times, heating the fuel in the process. This issue is especially significant when the rotational speed of the pump is high, and the engine fuel demand is low, for example during descent. This temperature increase thus limits the available cooling performance of the fuel. The total efficiency is also affected, as the amount of fuel pressurized may be many times larger than the amount of fuel actually used.

In this thesis, only recirculation back to the pump inlet is covered.

2.5.2 Flow control by variable displacement

The amount of fuel delivered can be set independently of the rotational speed of the pump if a variable displacement pump is employed, for example the axial piston pump covered in Sec. 2.4.2. This allows for exact control of the amount of fluid delivered, while at the same time avoiding a decrease in efficiency and excessive temperature rise. Possible downsides of these methods may include an increase in mechanical complexity and a weight penalty.

2.5.3 Flow control by throttling

A throttle valve can be used to restrict the discharge flow produced by a hydrodynamic pump by increasing the system resistance. This can be visualized by increasing the steepness of the system curve shown in Fig. 2.5, moving the point of operation to the left. This results in decreased flow rate and increased pressure build up upstream of the valve. This method offers a simple, lightweight method of controlling the amount of fuel delivered to the engine at various operating points. The throttle valve can be placed on the suction side of the pump, however this may cause low inlet pressures and thus cavitation in the pump. For this reason, the throttle valve is assumed to be placed after the pump outlet.

This method does however have downsides. By moving the point of operation to the right, the fuel pressure is increased. This additional increase in pressure is essentially wasted work. Furthermore, the throttling may move the point of operation further away from the BEP.

2.5.4 Speed flow control

Speed flow control implies control by varying the pump shaft rotational speed independent of the NH. This allows for precise control of the delivered flow, and may be utilized with both hydrodynamic rotary and hydrostatic displacement pumps. The main downside of this method originates from the need to use a variable speed transmission or an electric engine powered by a generator in order to control the shaft speed. This may significantly increase mechanical complexity, weight and decrease the power transfer efficiency between engine rotor and pump shaft. According to one of GKN's experts in electrical systems, a general constant transmission efficiency for mechanical systems can be assumed to be approximately 94 %, assuming a constant gear ratio. Likewise, a variable speed electrical system can be assumed to have a transmission efficiency of roughly 80 %, considering the combined efficiencies of the generator, power electronics, and the electrical motor powering a pump shaft.

2.6 Fuel properties

In order to properly estimate the behavior of the fuel system, some knowledge of the fuel properties is needed. The fuel used is assumed to be Jet A-1. Basic information regarding important properties is covered in this section.

2.6.1 Density, viscosity and specific heat capacity

The density, viscosity and specific heat capacity of the fuel all vary depending on the temperature and to a lesser extent pressure. The data used to estimate these properties are derived from [25, 26].

As the fuel temperature is expected to be well below the critical temperature, and since no vapour is assumed to be present in the liquid, the density, viscosity and specific heat capacity is assumed to be adequately described using only temperature correlations. The actual correlations used are described in Sec. 3.1.

2.6.2 Joule-Thomson coefficient

The Joule-Thomson coefficient, μ_{JT}, is defined as the rate of change of temperature with respect to the pressure at a constant enthalpy, or:

$$\mu_{JT} = \left(\frac{\partial T}{\partial p}\right)_h \tag{2.20}$$

This coefficient is needed when estimating temperature changes over valves, assuming the process can be considered adiabatic. The Joule-Thomson coefficient is also needed when assessing which parts of the total temperature change through a pump

is due to pumping inefficiencies or simply the temperature change due to compression, as described in [27].

The Joule-Thomson coefficient can also be expressed in the following manner, according to [28]:

$$\mu_{JT} = \frac{1}{c_p}\left(T\left(\frac{\partial V}{\partial T}\right)_p - V\right) \tag{2.21}$$

where c_p is the specific heat capacity at constant pressure, V is the specific volume, and $\left(\frac{\partial V}{\partial T}\right)_p$ is the coefficient of thermal expansion. By entering approximate values into Eqn. 2.21, a negative value is obtained. This indicates that the fuel should increase in temperature when expanded at constant enthalpy, for example when expanded over a valve, and decrease in temperature when compressed at constant enthalpy.

A correlation for the Joule-Thomson coefficient was established experimentally, as described in Sec. 3.4.

3
Methods

3.1 Estimation of density, viscosity and specific heat capacity

Two assumptions are made regarding the fuel properties.

- It is assumed that the LP stage is able to pressurize the fuel in such a manner that no vapor is present due to cavitation.
- The fuel temperature should never approach the critical temperature of the fuel.

Given these assumptions, pressure is assumed to have a negligible effect on the fuel properties.

Multiple linear density vs. temperature correlations from multiple sources within the span of -40 °C to 100 °C is listed in [25]. The source also contains older pressure vs. temperature data. While the overall behavior of the fuel density with regards to the temperature is similar in old and new data, the absolute values may differ somewhat, as the fuel cut included in different fuel type specifications may have changed over time. This data indicates that the density of jet fuel in general continues to vary in a linear manner with the temperature beyond 100 °C, at least until a temperature of 200 °C. Eqn. 3.1, obtained from [26], was used to approximate the density of Jet A-1 fuel as a function of the temperature in °C.

$$\rho = -0.8111 \cdot T[^{\circ}\mathrm{C}] + 814.1 \quad [\mathrm{kg/m^3}] \tag{3.1}$$

Similarly, the specific heat capacity at constant pressure was estimated using a linear correlation. The linear correlations differ somewhat, however the correlation in Eqn. 3.2 obtained from [25] is used, as it coincides well with data for Jet A-1 from [26], and has a similar slope to other Jet A-1 data listed in [25]. The data used to create the correlation range from about -10 °C to 160 °C.

$$c_p = 0.00428 \cdot T[\mathrm{K}] + 0.723 \quad [\mathrm{kJ/(kg{\cdot}K)}] \tag{3.2}$$

The kinematic viscosity of jet fuel does not vary linearly with temperature, however it should not be affected by pressure unless it approach the critical temperature as stated in [25]. The kinematic viscosity is estimated using plot data from [26] in the

temperature range -17 °C to 144 °C.

The dynamic viscosity is estimated by multiplying the kinematic viscosity with the estimated density. The extracted plot data used to calculate the kinematic viscosity is shown in Fig. 3.1.

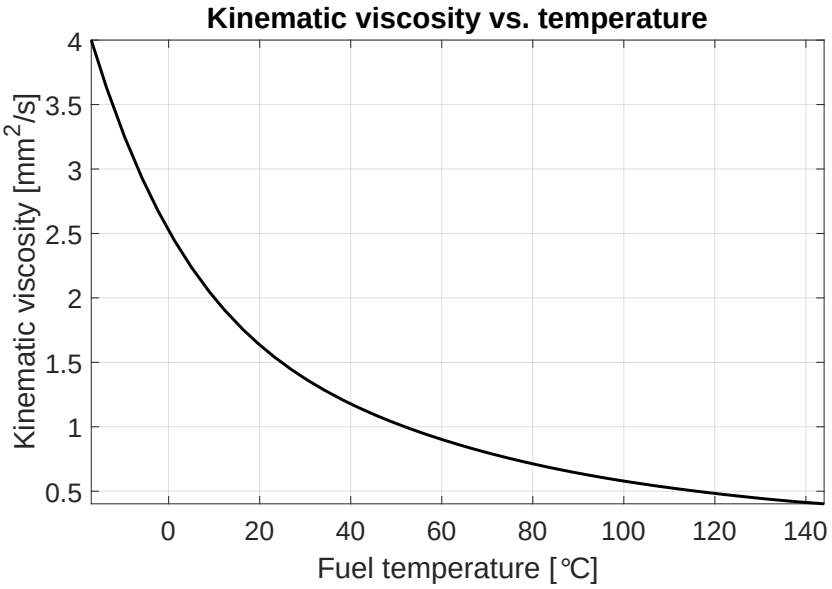

Figure 3.1: Extracted kinematic viscocity data for Jet A-1. Derived from [26].

3.2 Selection of model inputs

In order to estimate the behavior of the MFP, data derived using an engine performance model is used. The data supplied by the performance model consists of multiple engine values (e.g. pressures, temperatures, rotor speeds, mass flows) at different operating points for several defined simulated flight missions. The simulated flight missions are representative to typical flight data. The inputs to the MFP model must thus be limited to the variables that can be supplied by the engine performance model. Furthermore, the data supplied by the engine performance model may be limited in range depending on what operational conditions it is evaluated for. The range of data supplied by the performance model to the MFP model is therefore investigated, as it may limit the amount of test data needed to create the MFP model.

The necessary inputs to the MFP model given by the performance data is limited to the weighted fuel main (WFM), weighted fuel reheat (WFR) and NH. WFM is the mass flow rate to the main combustion chamber, and WFR is the mass flow rate to the A/B. However, in order to describe the MFP behavior, the inlet pressure and temperature, as well as the required MFP outlet fuel pressure and servo leakage mass flow is needed.

While the required MFP outlet fuel pressure can be estimated based on the WFM

using data from uninstalled engine tests, the servo leakage flow rate as well as inlet pressure and temperature is currently unavailable. These inputs therefore need to be estimated when running the MFP model.

The operational limits of the inputs is covered in detail in Sec. 3.3.2.

3.3 Data collection

This section covers motivations and description of data collected from rig tests used to formulate the model. A description of the test rig is also included.

3.3.1 Test rig description

A test rig normally used for acceptance testing of overhauled MFP units or serviced MFP units was used to gather test data. An electric motor in the test rig will drive the MFP at the desired rotational speed. In addition, valves in the rig are used to control the volumetric flow rate and pressure levels in different parts of the system. In this way, operating conditions can be set to mirror conditions present during actual operation. The fluid used in the test rig flow in a closed loop. Fluid is drawn from a large tank, passed through the MFP and a cooler and subsequently returned to the tank. The cooler combined with the large volume of the tank ensure near constant MFP fluid inlet temperatures, however there is no possibility of precisely controlling the MFP inlet temperature, and is thus dependent on the ambient conditions. The test rig contain several sensors sampling several times per second. This data includes rotational speed, pressure levels, volumetric flow rates and temperatures in multiple areas of the system. For a schematic overview of the test rig, see Fig. 3.2.

The test rig is specified to operate using MIL-C-7024 type II fuel system calibration fluid. While no correlations of the property behavior was available other than density and viscosity at ambient conditions it is assumed that the properties of this fluid closely resemble the properties of Jet A fuel in general. It was therefore assumed that the data gathered using this fluid should be very similar to the hypothetical data generated had Jet A-1 been used.

3.3.2 Formulation of test matrix

A test matrix was constructed for a custom rig test. The purpose of the custom rig test was to gather steady state data at operational points not normally investigated. This data was used, in addition with previously collected data from routine test rig operation, as a basis for the MFP model. In order to construct a representable test matrix, the operational limits of the input data was investigated. Since the behavior of the MFP was to be investigated both with and without activated A/B, the test data was segregated based on the presence of A/B activation. For the data

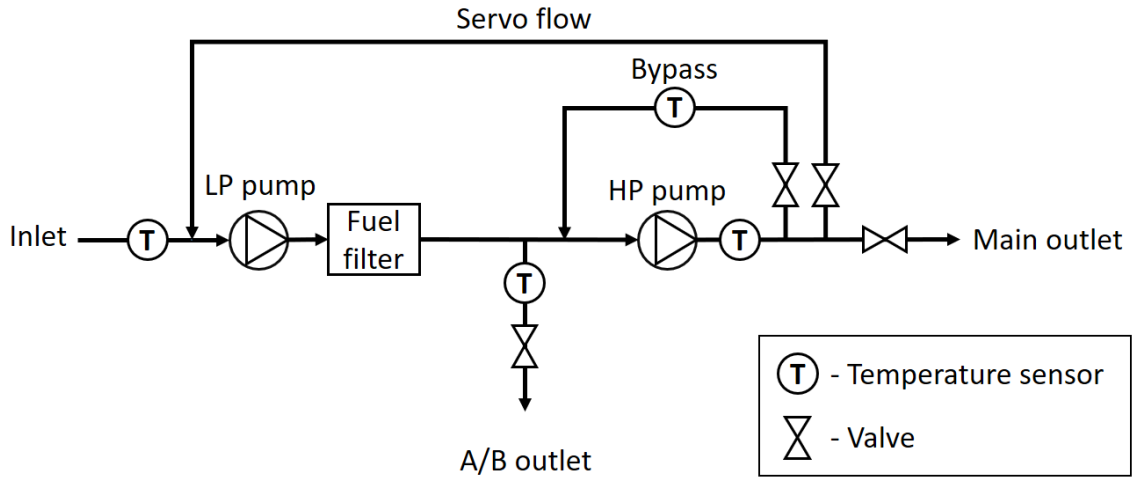

Figure 3.2: Functional schematic of the test rig. Pressure and flow sensors are omitted from the image.

containing no A/B activation, test points were selected according to the first image in Fig. 3.3. Effort was made to properly cover the entire operational area. Likewise, the test points selected for the data with A/B activation can be seen in the second image of Fig. 3.3. Here, a suitable WFR was selected based upon the chosen WFM. Correlations for the maximum and minimum WFR and WFM values was established for the relevant range in NH. Linear interpolation between maximum and minimum WFM, given a chosen test WFM was used to predict a suitable WFR value. This was done in order to cover the majority of the operational area with as few test points as possible. Thus, each single green point (WFM) in the second image of Fig. 3.3 correspond to a single yellow point (WFR) for every test point. Notice that the mass flow rate on the y-axis has been normalized, in this case by the maximum inlet mass flow present in the data supplied by the performance model. The rotational speed is given as a percentage of NH. In total 26 test points were selected.

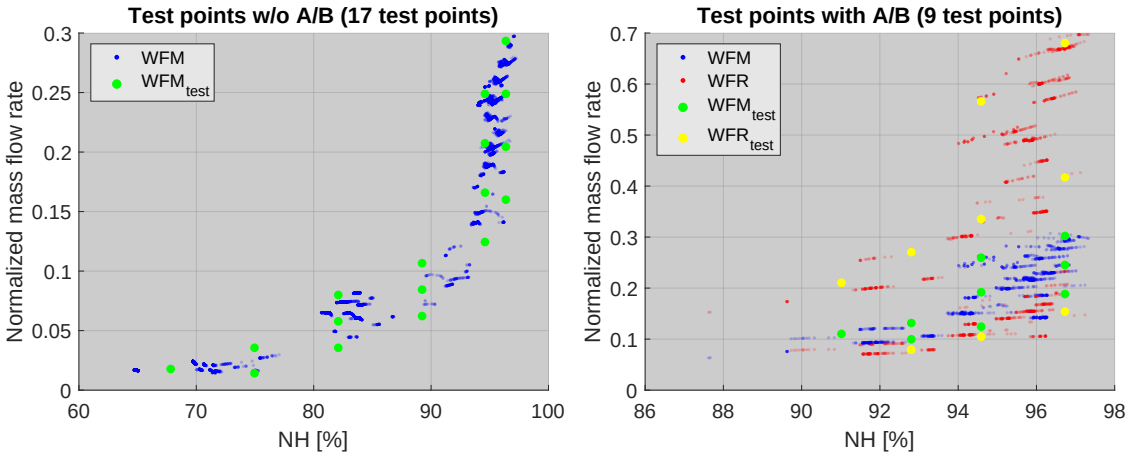

Figure 3.3: Visualization of test matrix selection of NH, WFM and WFR, with and without A/B flow.

A suitable outlet pressure was selected based on the WFM using a correlation de-

rived from uninstalled engine tests. The normalized correlation is shown in Fig. 3.4 for illustrative purposes.

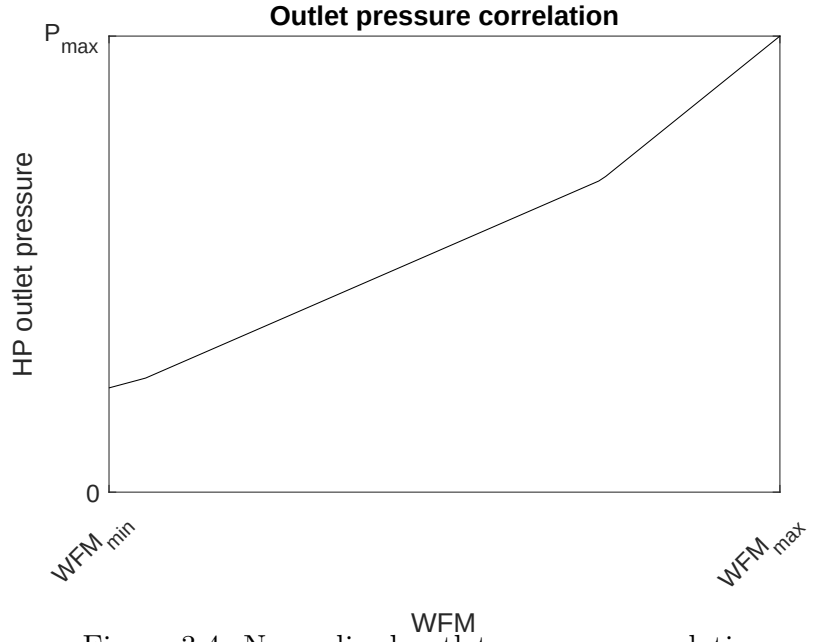

Figure 3.4: Normalized outlet pressure correlation.

As the temperature between the LP and HP stages was needed in order to establish efficiencies, a small amount of fluid was allowed to exit through the A/B outlet at test points defined at no A/B activation. This was done to avoid stagnant fluid at the temperature sensor placed in the A/B channel, therefore ensuring an accurate temperature measurement after the LP pump and fuel filter. Furthermore, since there is no temperature sensor in the servo flow channel, the servo flow channel valve was completely closed so as to not introduce uncertainties in the temperature measurement of the fluid entering the LP pump.

3.3.3 Description of collected data

In total, 26 test points were evaluated in the test rig. Each test point was run until no noticeable temperature change was perceived in the A/B channel temperature sensor, to ensure steady state conditions. This resulted in an approximate mean runtime of 2 minutes per test point.

Due to limitations in the test rig, the HP stage outlet pressure could not be set to desired levels at some operating points. Specifically, the pressure at low flow conditions could not be set sufficiently low. Furthermore, some temperature change was still present for some test points at temperature sensors located in the HP region of the MFP.

Temperature, volume flow rate and pressure data was collected for the test points at all available sensor locations of the system. By studying the temperatures and

volume flow rates in the oil cooling loop connected to the pump bearings, it was determined that the heat energy leaving the system was negligible compared to the heat energy supplied to the fuel.

3.4 Identification of Joule-Thomson coefficient

A correlation for the Joule-Thomson coefficient was established using the temperature and pressure measurements upstream and downstream of the bypass valve, assuming adiabatic expansion at data points deemed steady state from the custom rig test. The result can be seen in Fig. 3.5.

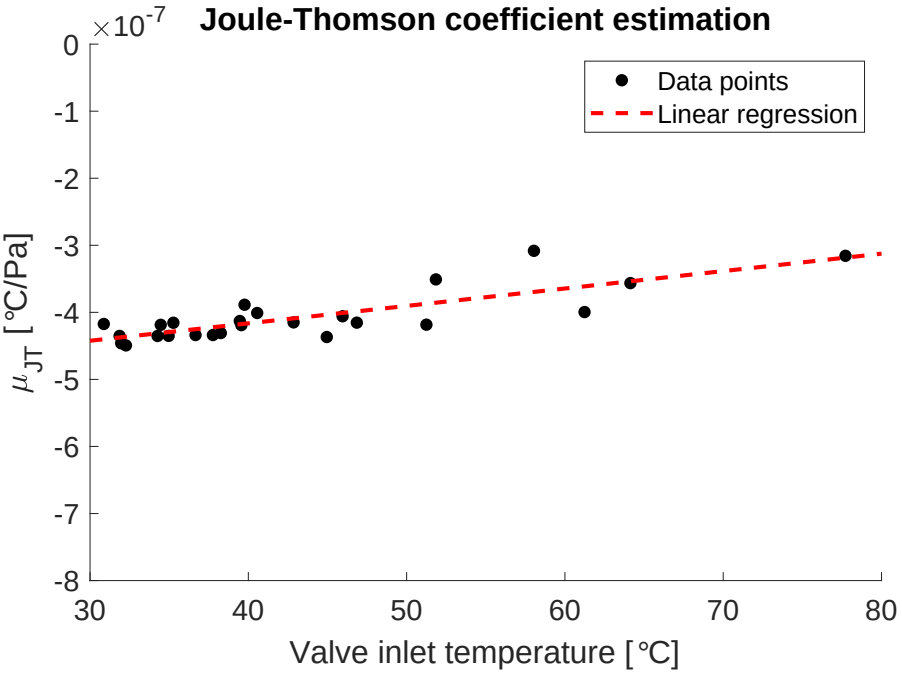

Figure 3.5: Estimation of the Joule-Thomson coefficient function using linear regression, expressed as a function of the inlet temperature at the bypass valve.

The value of the Joule-Thomson coefficient is negative as expected. The linear regression equation is shown in Eqn. 3.3.

$$\mu_{JT} = (2.5972E-9) \cdot \mathrm{T_{inlet}}[°\mathrm{C}] - 5.2027E-7 \ [°\mathrm{C/Pa}] \tag{3.3}$$

3.5 Identification of LP stage head and efficiency curve

To define the LP-stage behavior, work was conducted to express the LP pump and filter dimensionless head and total efficiency curves, assuming fully turbulent flow

and dynamic similarity at all operational points.

The efficiency was estimated at the steady state data points gathered from the custom rig test using Eqn. 2.9. Having defined an expression for the Joule-Thomson coefficient, the estimated temperature change due to compression could be removed from the total temperature change over the LP stage ($\Delta T_{\text{pump}} = \Delta T_{\text{total}} - \Delta T_{\text{compression}}$). The temperature change used to calculate the total efficiency of the LP stage could thus be estimated using only the estimated temperature rise due to pumping inefficiencies. Similarly, a head coefficient curve was created. In this case, data from routine operation was used, as it contained a greater amount of steady state data.

Fig. 3.6 shows the estimated head coefficient and efficiency curves as a function of the flow coefficient, using rotational speed in rotations per second.

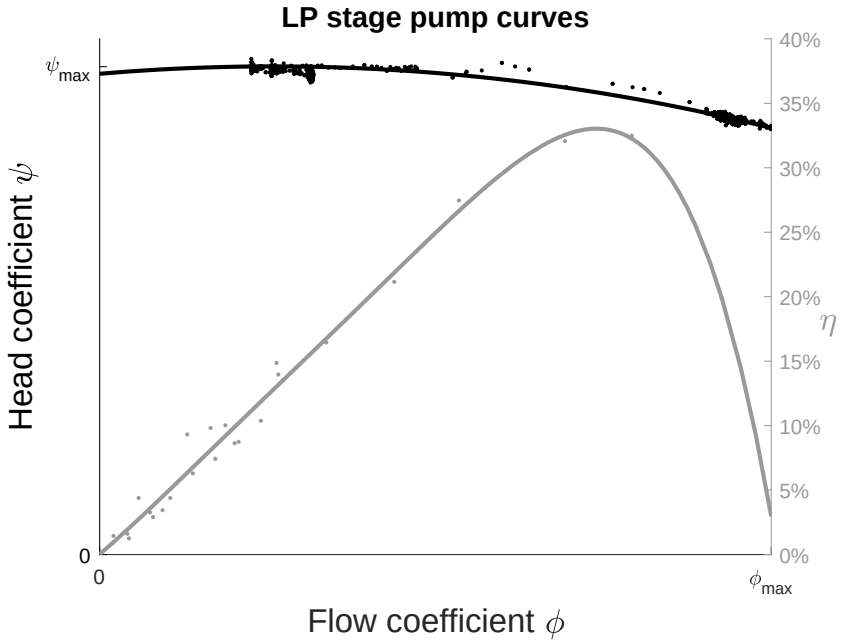

Figure 3.6: LP stage pump curves with data points.

3.6 Identification of HP stage volumetric efficiency

Due to the limitations in the test rig described in Sec. 3.3.3, it was not possible to accurately describe the total efficiency of the HP pump using only temperature and pressure measurements. However, since the ideal displacement per rotation of the gear pump was known, it was possible to create an estimation of the volumetric efficiency based on volume flow rate measurements at different rotational speeds from data collected from the custom rig test, as well as data generated during routine operation. By relating the HP pump efficiency to the Stribeck number the correlation shown in Fig. 3.7 was created. Note that the estimated volumetric efficiency points

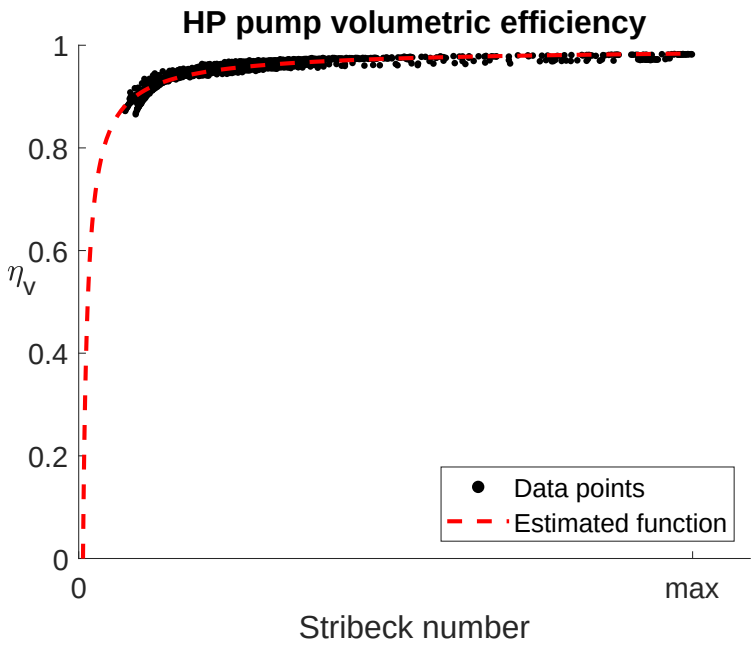

Figure 3.7: HP stage volumetric efficiency.

closely adhere to the typical volumetric efficiency curve shape as described in [13].

3.7 RM12 state estimator formulation

A state estimator for the RM12 was created using MATLAB. A functional flow chart of the script can be seen in Fig. 3.8.

The code uses WFM, WFR, and NH as specified by a performance model, as well as estimations of inlet pressure, temperature and servo leakage mass flow as inputs. The script operates iteratively until the temperatures in the system converge. First, pressures and volume flow rates are estimated. These estimations are subsequently used in combination with efficiency models to estimate temperatures in the system. As the temperatures changes, fuel, pump, and valve behavior changes. The code must therefore iterate in order to update both pressures and temperatures as their behaviors are coupled.

3.7.1 Calibration of model using HP total efficiency

As the total efficiency of the HP stage gear pump could not be evaluated using data derived from the custom rig test, uninstalled engine test data was instead used to calibrate the gear pump total efficiency. The data contained values such as WFM, WFR, NH, inlet temperatures and pressures as well as temperatures and pressures at both A/B and main outlets. However, an estimation of the servo leakage mass

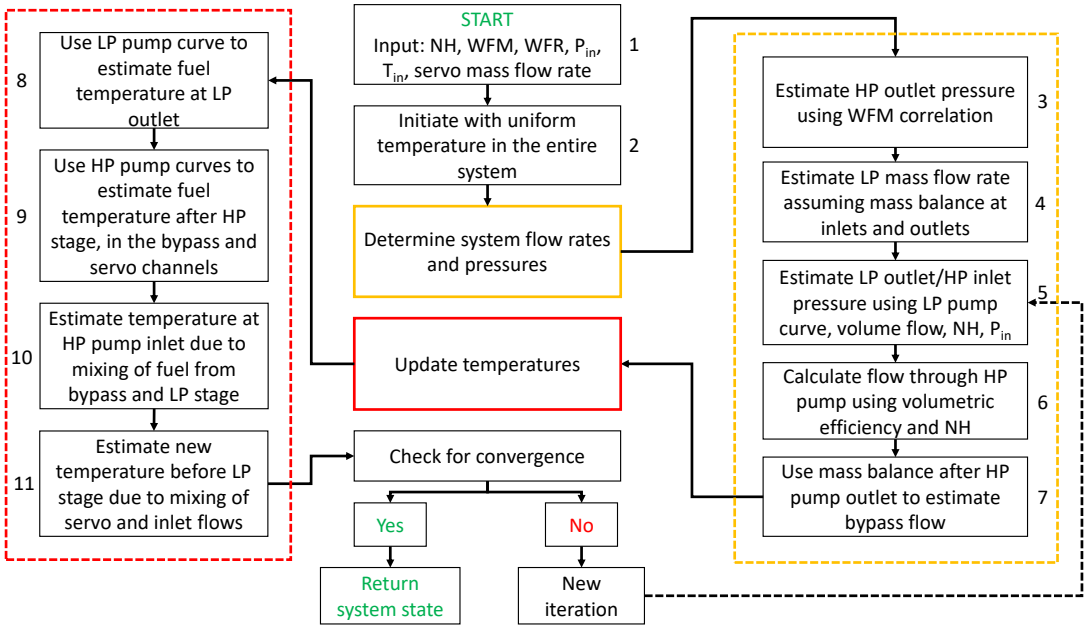

Figure 3.8: State estimator code flow chart.

flow rate was based on ABC and MFC specifications as it was not included in the engine test data.

The state estimator model was calibrated using the uninstalled engine test data as inputs. By matching the derived outlet temperatures to the outlet temperatures supplied by the engine model, using the HP gear pump mechanical efficiency, the total efficiency could be estimated for each point. In total 20 test data points were used.

It was found that when the points were plotted against the Stribeck number, the mechanical and total efficiency did not follow the typical function shape as described in [13]. Instead, the pressure differential and the rotational speed of the pump was found to be a better measure for correlating the efficiency. An estimated curve of the total efficiency curve as a function of the differential pressure times the rotational speed of the pump (in radians per second) was established by simply drawing straight lines between points. The data points and total efficiency estimation curve is shown in Fig. 3.9. Note that while most points are placed in close proximity to the line, four points in the right side of the image are placed considerably further away. These lines corresponds to high engine flows, with and without A/B activation, and thus a small amount of bypass flow. The estimation line was placed in between these points in an effort to avoid overfitting. While these points are placed relatively far away from the estimated curve, the resulting outlet temperatures using the estimated curve are within 2 °C of the outlet temperature supplied by the uninstalled engine data at these points. Possible explanations for the efficiency behavior of the HP stage gear pump are discussed in Sec. 5.3.

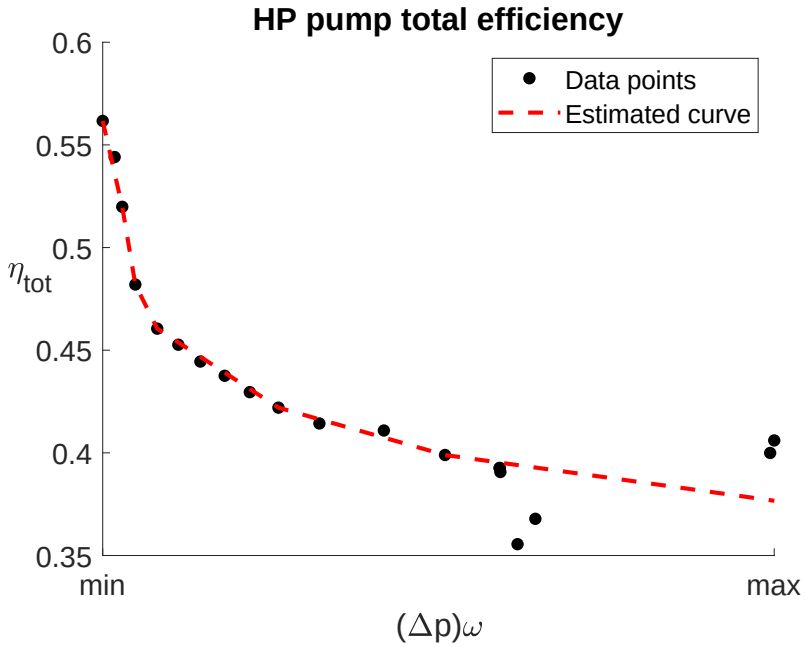

Figure 3.9: HP stage total efficiency.

3.8 Selection and implementation of alternative MFP architectures

Having established a model for the baseline RM12 system, 3 alternative systems were selected for implementation. The selected systems are described in this section, along with brief motivations for their selection. Descriptions of their implementations in code as well as a brief comparison of characteristics is discussed.

3.8.1 System with centrifugal HP stage pump

By replacing the HP gear pump with a centrifugal pump rotating at a higher speed and controlling the flow with a throttle valve, it may be possible to decrease the total weight of the system, as the pump diameter can be made considerably smaller at higher rotational speeds. A maximum pump shaft rotational speed of 30 000 RPM was estimated using information from [17]. As the pumps need to be able to supply adequate pressure at the maximum engine flow, the pressure and flow required at this operational point was used to calculate the specific speed of the HP pump stage. The estimated specific speed, using the same definition as shown in Fig. 2.8 was estimated to be about 16. This number indicates that a partial emission pump can be used. However, if two stages are used the specific speed for each stage is approximately 27. This number indicates that a dual-stage radial centrifugal pump can be used at a much smaller specific diameter. As more data is available on the behavior of conventional radial centrifugal pumps it was decided to use a two stage

radial centrifugal pump. A maximum total efficiency of 50% was assumed based on Fig. 2.8. Pump curve shapes were estimated using pump curves shown in Fig. 2.13. The BEP was assumed to be located at maximum engine flow and pressure. The resulting estimated dimensionless pump curves can be seen in Fig. 3.10.

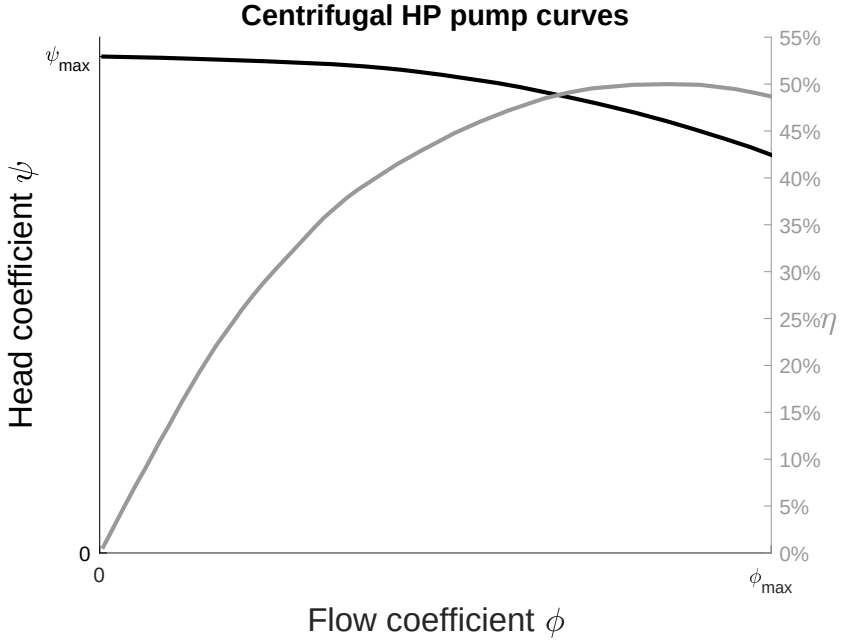

Figure 3.10: Dimensionless centrifugal HP pump curves.

In essence, this alternative system uses the baseline centrifugal RM12 low pressure stage with a separate high speed shaft driving a dual-stage centrifugal HP pump. As this system does not utilize a displacement pump in the MFP, the rotational speed can be increased, however a separate smaller displacement pump needs to be used in order to prime and supply sufficient flow and pressure at low rotational speeds. However, if fuel is used as hydraulic fluid on engine actuation systems, it may be possible to use a single pump for both actuation and priming purposes, thereby reducing the potential weight penalty needed to ensure low rotational speed function. Additionally the use of centrifugal pumps instead of displacement pumps avoid the use of metal-to-metal contact surfaces, which may increase component life expectancy and thereby reduce operational cost.

This alternative was implemented similarly to the RM12 system, with some minor differences. The volumetric flow to the engine was simply set to match the engine requirement, and the additional pressure generated at this point was expanded after the pump to the pressure required by the engine. The bypass channel was also removed.

3.8.2 System with axial piston HP stage pump

Another concept utilize a variable axial piston pump instead of a gear pump in the high pressure stage of the baseline RM12 system. The piston pump is assumed to rotate at the same rotational speed as the baseline HP pump. By using this type of pump the flow and pressure to the engine can be set to match the engine requirement without the use of a bypass or throttle valve, at the cost of increased mechanical complexity, and possibly a slight increase in weight. The increase in mechanical complexity may increase cost and reduce reliability.

In order to create an estimation of the total efficiency of the axial piston pump, open total efficiency data was collected from a multitude of axial piston pumps using catalogues published by the pump manufacturer Parker [29, 30]. Estimations of the efficiency behavior depending on the Stribeck number was established for this data. It was assumed that the maximum total efficiency should not rise beyond 80%. A basic estimation of the total efficiency curve was created using the same equation form as shown in [14]. The equation was altered to peak at a total efficiency of 80%, with a downward slope similar to the data gathered from [29] and [30]. The peak efficiency point was placed at a Stribeck number roughly in between the points of peak efficiency given by the data points derived from the catalogues and the empirically determined curve for the piston motor derived in [14]. The resulting total efficiency curve and data extracted from the catalogues can be seen in Fig. 3.11.

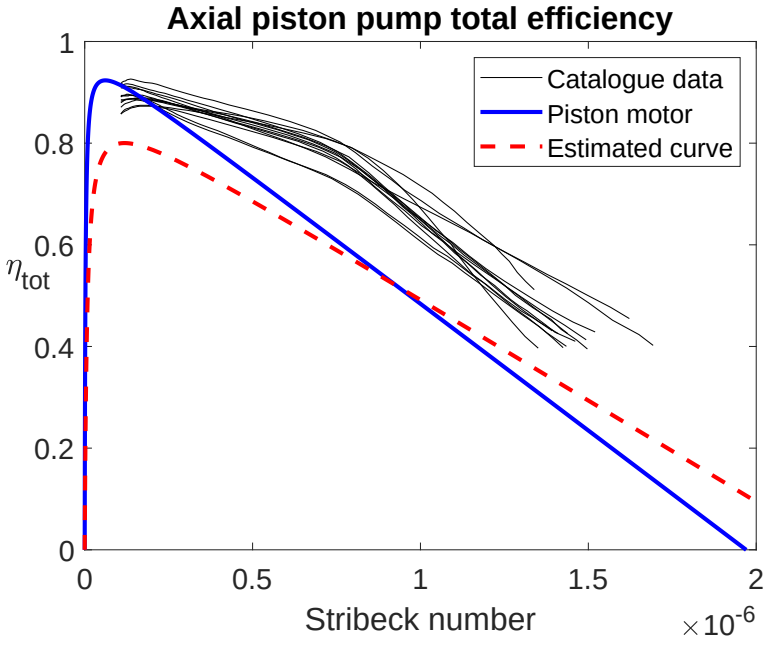

Figure 3.11: Axial piston pump total efficiency.

The axial piston pump was implemented in a similar way to the previously described centrifugal HP pump system, however no throttling valve was used as the generated

pressure and flow should match the required engine conditions.

3.8.3 Electrically driven system with centrifugal stages

The final concept controls the flow by changing the speed of the pump. In this case, an electrical system is used to power the pumping system at speeds up to 30 000 RPM. The concept utilizes centrifugal pumps at both the LP and HP stages, mounted on a common shaft. The HP pump is identical to the HP centrifugal pump described in Sec. 3.8.1 as the maximum pressure, flow and rotational speed are the same in both concepts. The LP stage uses pump curves derived in a similar manner as the HP centrifugal pump. The result can be seen in Fig. 3.12. Note that this curve is a general description. A fuel filter is not included in this curve, and thus for an actual case the pump curve behavior would be somewhat different.

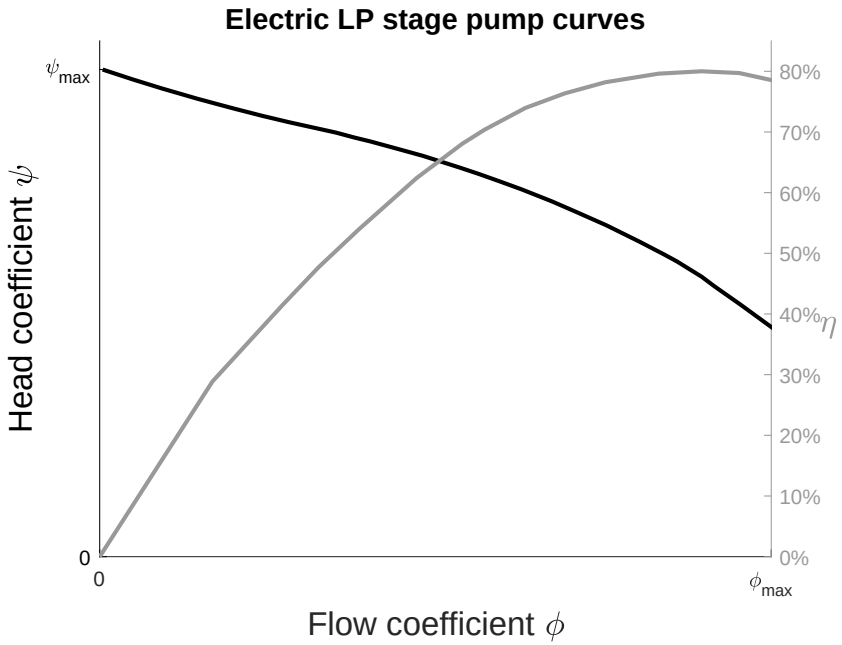

Figure 3.12: Dimensionless electrically driven centrifugal LP stage pump curves.

In this case a specific speed of about 140 (using the same definition as shown in Fig. 2.8) was derived, assuming maximum pressure at maximum flow, also placing the BEP at that point. By changing the pump shaft rotational speed, the pumps can be set to directly generate the required flow and pressure, avoiding losses in efficiency due to excess pressure buildup. As the pump shaft rotational speed can be controlled independently of the NH, the centrifugal pumps are able to supply sufficient pressure even at low NH. There is also a possibility that the centrifugal stages may be able to prime the system. Because of these reasons, it may be possible to disregard the use of a displacement pump for starting and priming purposes. Possible system downsides include increased weight, cost, and possibly reliability, as

a result of the use of power electronics.

The implementation of this concept closely matches the implementation of the previous system with a centrifugal HP stage pump, however for each input operational point an iterative method (Newton's method) is used to estimate the rotational speed needed to precisely match the engine requirement at the HP pump outlet.

4
Results

4.1 Comparison of fuel systems configurations

When comparing fuel systems configurations, three key flight operating points are of interest: flight idle (FI), intermediate rated power (IRP), and maximum A/B thrust (MT). FI refers to the minimum thrust the engine can maintain in flight to keep the aircraft operational. FI conditions typically occur at A/C speed reduction and descent. IRP refers to maximum engine thrust without A/B activation. MT refers to maximum engine thrust with A/B activation.

Descriptions of the four different system configurations investigated are presented in Tab. 4.1. These are the same systems described in Sec. 3.8 as well as the baseline RM12 system. Brief descriptions are included along with a numbering system used for clarity.

Table 4.1: Fuel system numbering description.

System 1	Mechanically driven radial centrifugal LP pump and external gear HP pump with bypass (baseline RM12)
System 2	Mechanically driven radial centrifugal LP pump and axial swash plate piston HP pump w/o bypass
System 3	Mechanically driven radial centrifugal LP pump and double stage radial centrifugal HP pump with throttle valve
System 4	Electrically driven radial centrifugal LP pump and double stage radial centrifugal HP pump

System 1, System 2, and System 4 utilize a single shaft to drive both the LP and HP pumps. System 3 utilize two separate shafts to drive the LP and HP pumps respectively.

Plots of the MFP power usage, fuel temperature rise, driving energy, and cooling capacity comparisons between the four fuel system configurations are shown in this section. Furthermore, scatter plots relating volumetric bypass ratio to temperature increase, engine volumetric flow to throttle valve pressure levels, engine volumetric bypass ratio to pump shaft rotational speed and LP vs. HP temperature rise are presented.

All data presented in this section have been calculated assuming an inlet temperature of 42 °C, inlet pressure of 1 bar, and a constant servo leakage mass flow.

4.1.1 Power usage

Achieving a lower pump power usage is desirable, as all power consumption not transformed to useful hydraulic work (i.e. required flow at required pressure level) is considered a waste. Several power uses add to the total wasted work performed by the pump.

- Individual pump inefficiencies.
- Recirculation of fuel.
- Throttling of excess pressure.
- Efficiency of HP rotor to pump shaft power transmission

In Fig. 4.1, 4.2, and 4.3, each bar is adjusted with a corresponding transmission efficiency to obtain the corrected power extracted from the HP rotor to power the pumps. The horizontal line marked "useful power" denotes the pressure work between MFP inlet and outlets, including the outlet leading to the A/B, as well as the pressure work used in the servo channel. The derived useful power differs at most by 5 % between different systems. A single line denoting the mean value derived for all systems is therefore used, as it proved unhelpful to present several values.

4.1.2 Fuel temperature rise

The fuel temperature rise across a MFP is calculated by subtracting the main outlet temperature by the inlet temperature. This temperature rise is an indication of the system efficiency, as it correlates with work losses. Additionally, achieving a lower fuel temperature rise is desirable since the fuel can be used as a heat sink in later stages of the fuel system. The maximum fuel temperature rise for the 4 compared fuel systems are presented in Fig. 4.4.

4.1.3 Driving energy

A fuel system's driving energy is a measure of the total work extracted from the HP rotor to drive the MFP and indicates the pump total power use during a mission, and subsequently provides an indication of the effect on the SFC, ignoring additional factors such as added weight. The driving energy shown in Fig. 4.5 is calculated as a time integral of the power removed from the HP rotor over all missions included in the performance model. The plot is normalized by the driving energy of System 1.

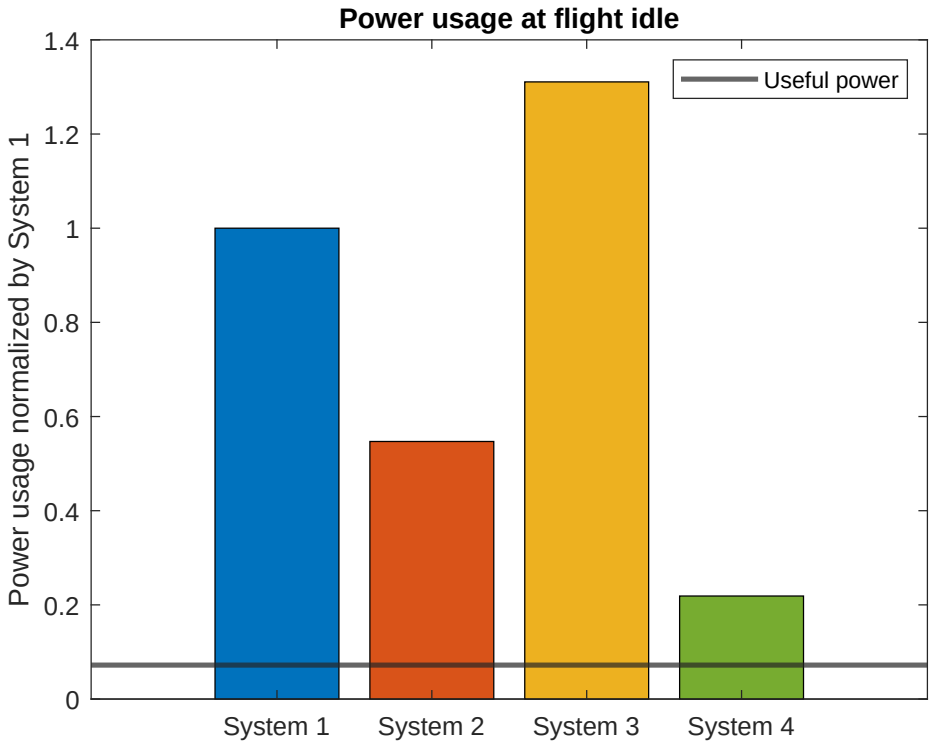

Figure 4.1: Bar plot of the MFP power usage at flight idle.

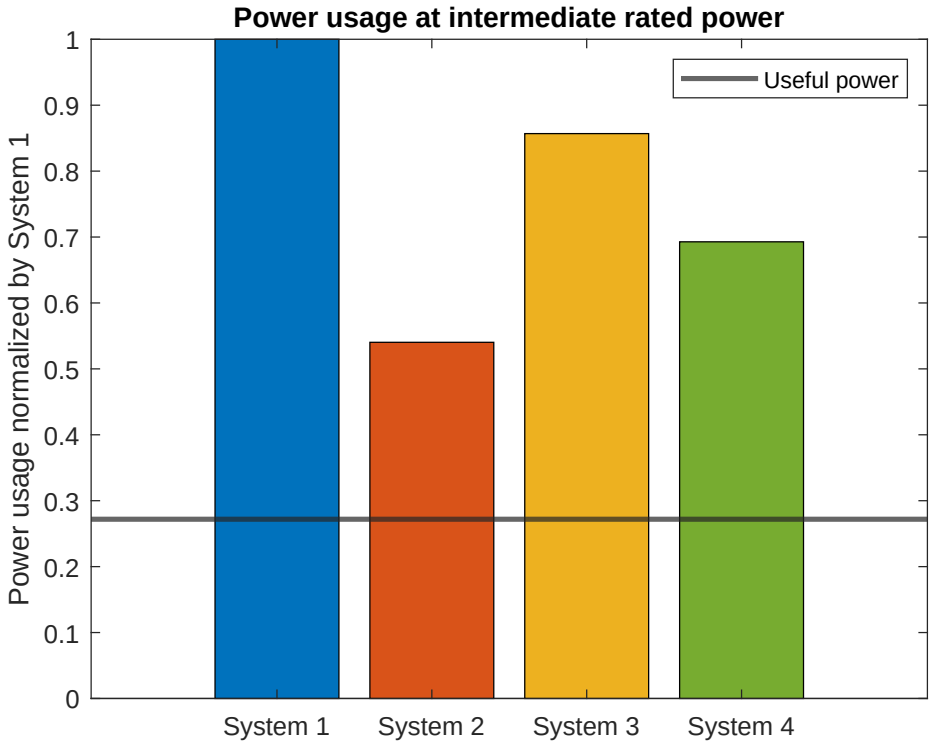

Figure 4.2: Bar plot of the MFP power usage at intermediate rated power.

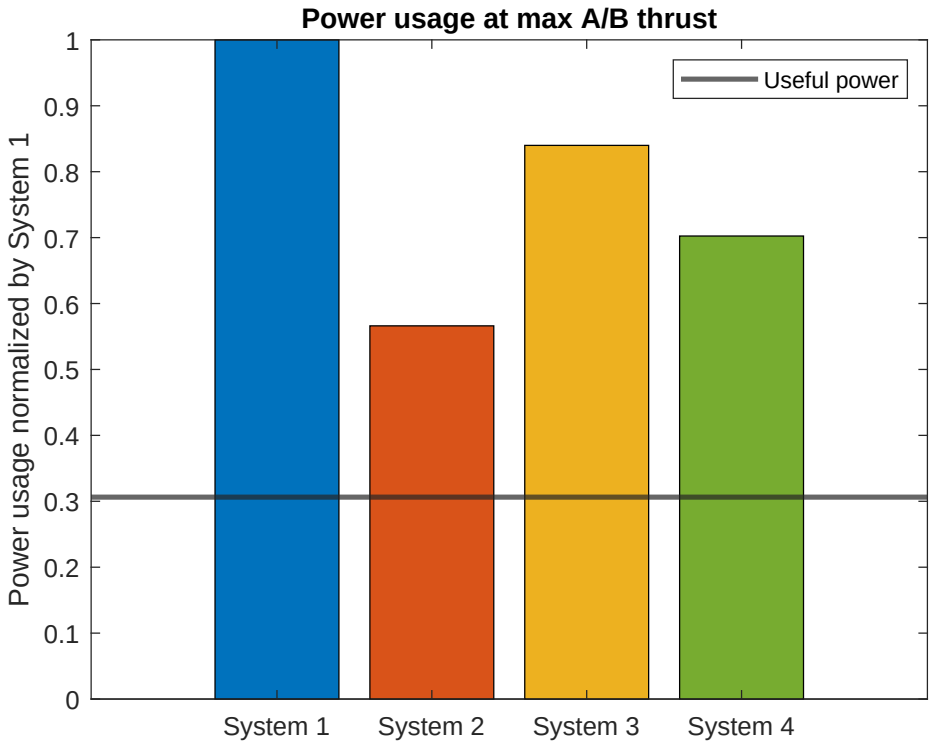

Figure 4.3: Bar plot of the MFP power usage at maximum A/B thrust.

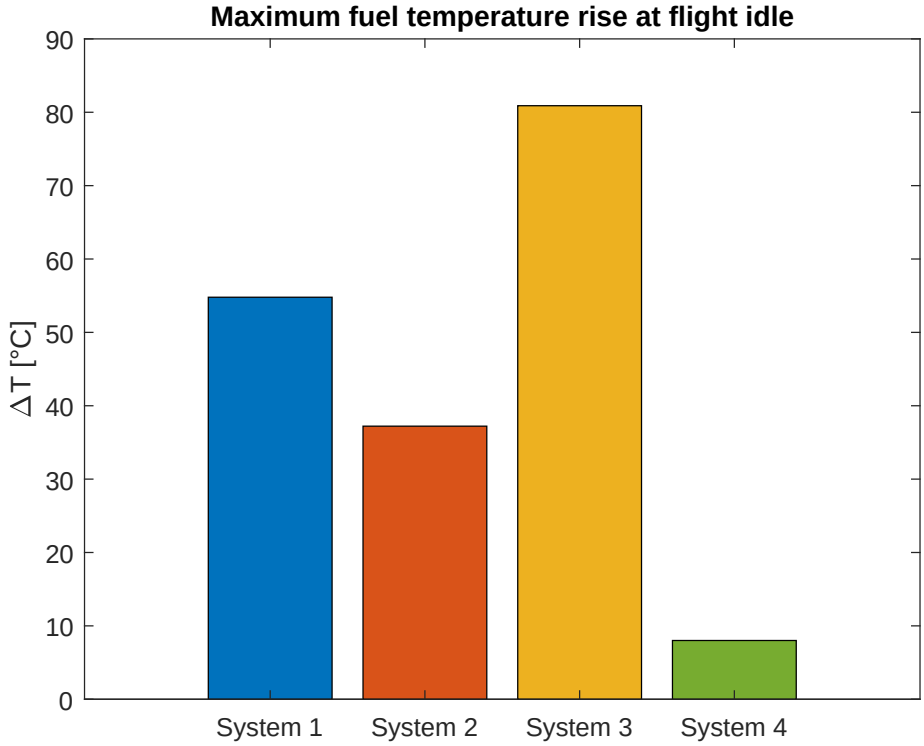

Figure 4.4: Bar plot of the fuel temperature rise over the MFP at flight idle.

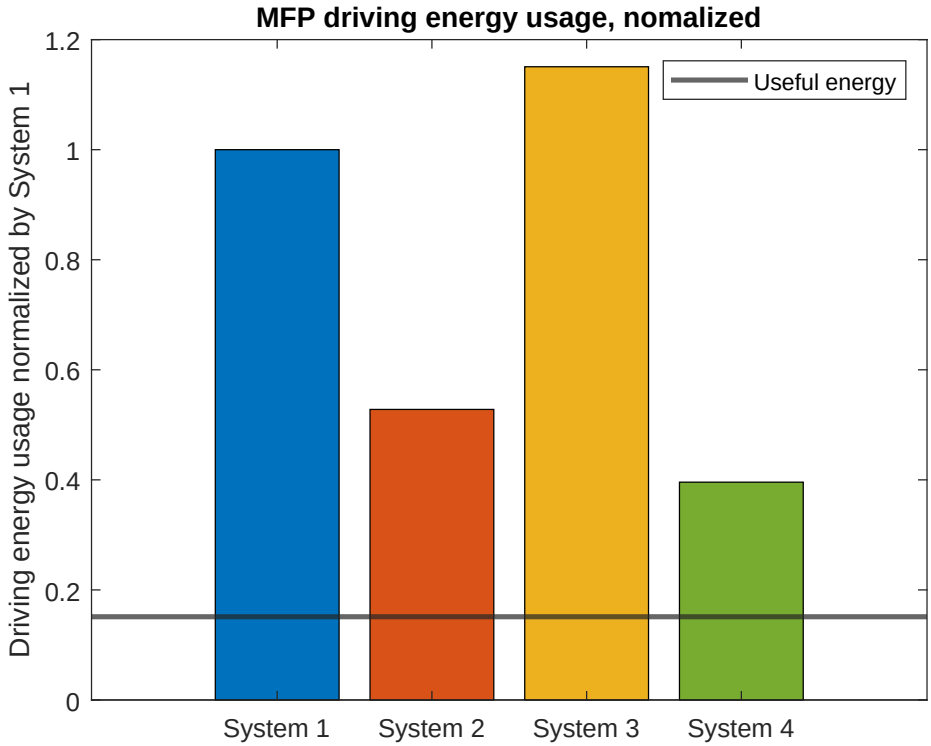

Figure 4.5: Bar plot of average MFP driving energy.

4.1.4 Cooling capacity

A fuel system's cooling capacity is a measure of a system's ability to act as a heat sink. The maximum allowed temperature the fuel can reach within a fuel system is assumed to be 150 °C. The cooling power available is calculated as in Eqn. 4.1.

$$\dot{Q} = \dot{m} c_p (T_{\max} - T) \tag{4.1}$$

Where $\dot{m}$ is the outlet mass flow, T and $T_{\max}$ is the outlet and maximum fuel temperature respectively. c_p is the fuel specific heat capacity, estimated as the average of the specific heat capacities evaluated at the outlet temperature and maximum temperature. Fig. 4.6 show the available cooling capacity of the fuel for each fuel system calculated as an integral of the cooling power over all flight conditions. The bars are normalized by the cooling capacity of System 1.

4.1.5 Temperature rise due to bypass ratio

The image shown in Fig. 4.7 is included to illustrate the clear connection between bypass ratio and temperature increase in System 1.

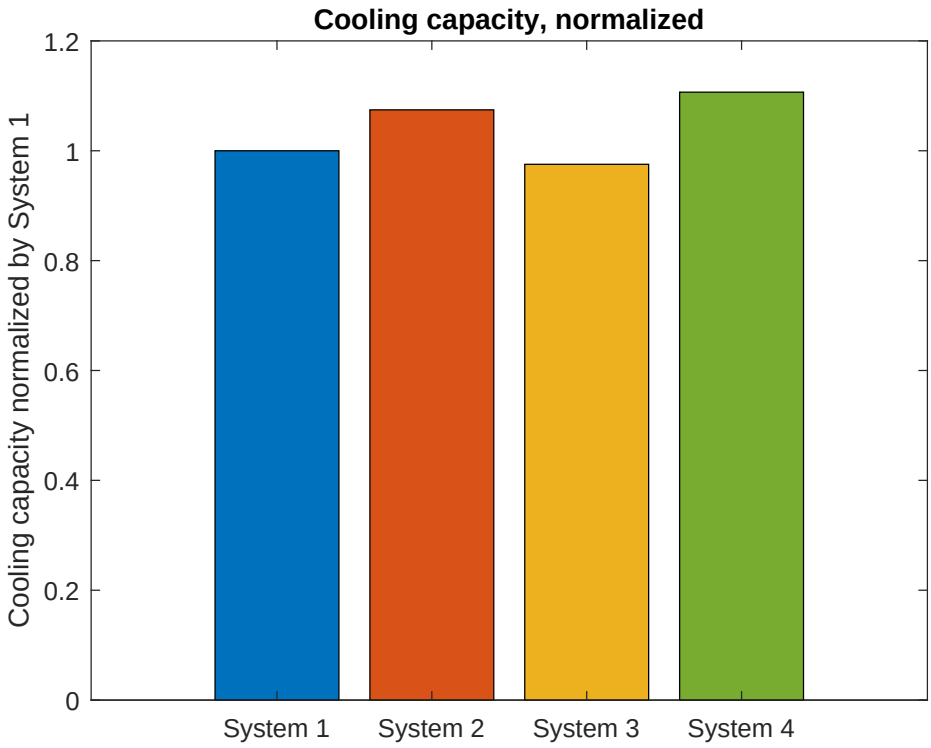

Figure 4.6: Bar plot of cooling capacity. Normalized by System 1.

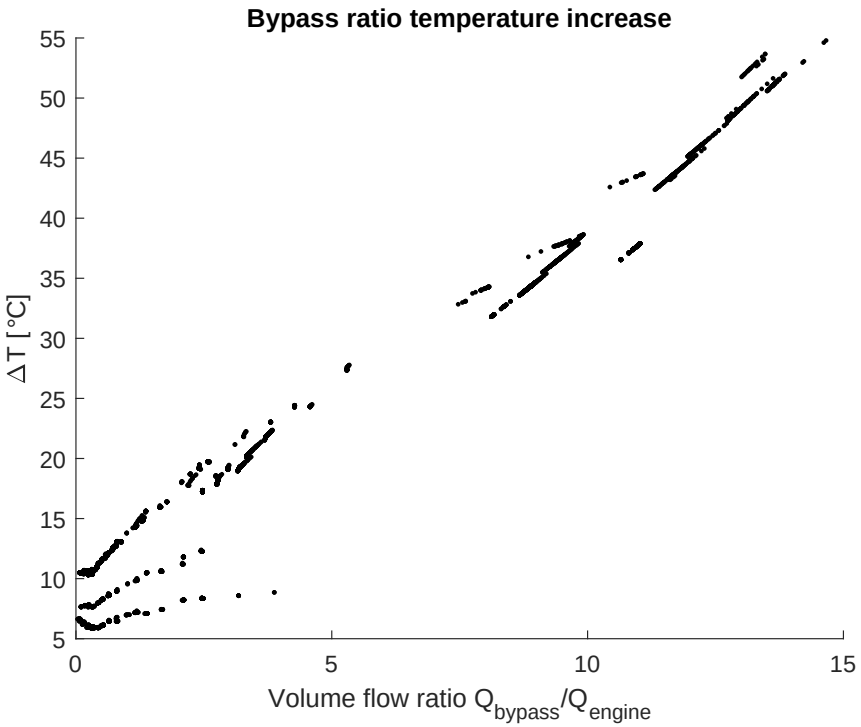

Figure 4.7: Scatter plot relating volumetric bypass ratio and temperature rise in System 1.

4.1.6 RM12 modeled LP vs. HP stage temperature rise

The temperature rise in the LP vs. the HP stage for the baseline System 1 can be seen in Fig. 4.8. This is included to demonstrate how the LP stage affect the total temperature increase depending on the bypass ratio. A value above 0.5 on the y-axis indicates a majority of the temperature increase comes from the LP stage. Additionally, 3 distinct lines can be seen. The decrease in temperature ratio corresponds to an increase in A/B fuel flow.

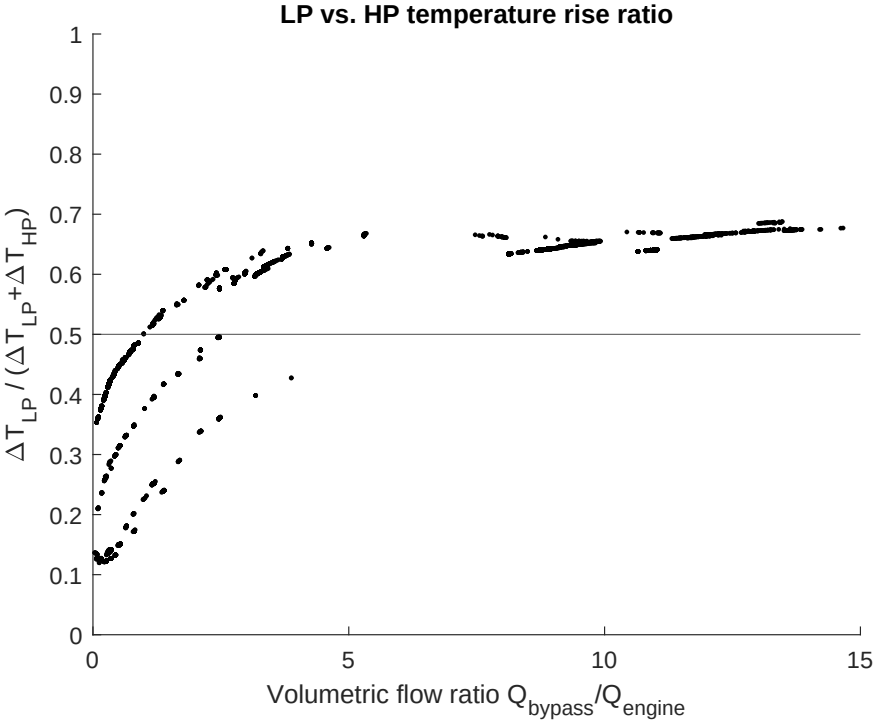

Figure 4.8: LP vs. HP stage temperature increase ratio as a function of the volumetric bypass ratio in System 1.

4.1.7 Throttle valve pressures

In Fig. 4.9 the pressure levels on both sides of the throttle valve, that is the generated pressure and the required engine pressure is shown as a function of the volumetric engine flow. The difference between the generated pressure and the pressure required by the system is essentially wasted energy, which helps explain why System 3 exhibits a poor overall efficiency at low engine fuel flows.

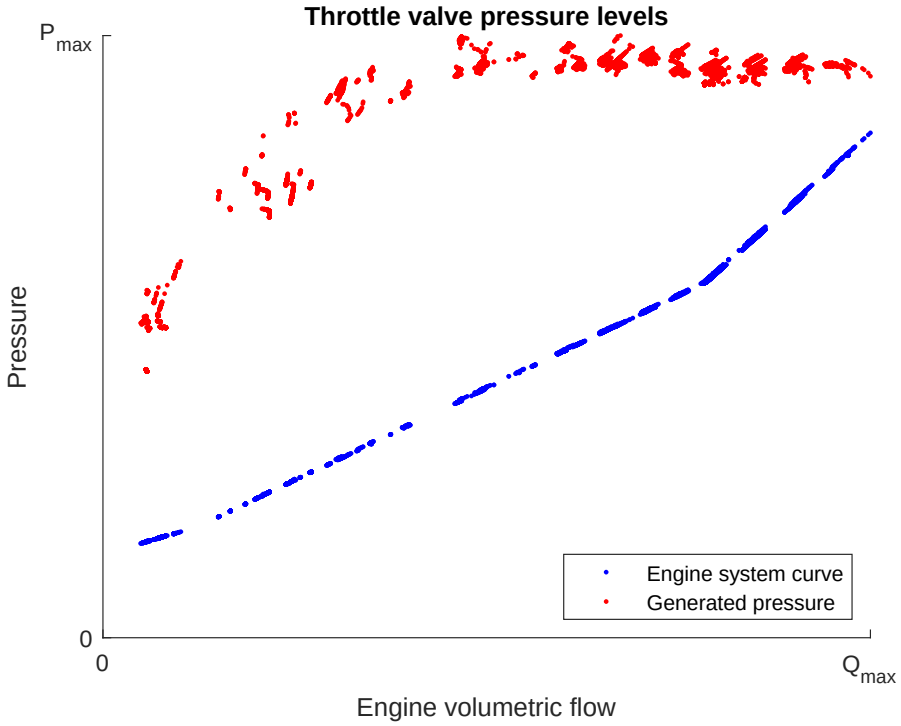

Figure 4.9: Pressure levels before and after the throttle valve in System 3.

4.1.8 Electric speed control

In contrast to System 3, System 4 change the rotational speed of the pump shaft in order to match the engine requirements. Fig. 4.10 shows how the rotational speed changes depending on the engine volumetric flow requirement. The NH is also shown as a percentage of the maximum speed. Note that at low engine volumetric flows, the electrically driven pump spins at about one third of the maximum rotational speed, whereas a pump using a mechanical transmission and constant gear ratio would spin at about 70 % of the maximum speed.

4.2 Further comparison of fuel system characteristics

To further evaluate one A/C fuel system against another, an extended comparison must consider factors such as penalties of adding weight to a system, reliability problems, cost, and more. Tab. 4.2 presents a brief and estimated comparison of the systems based of these parameters alone. Further studies has to be done in this area.

Cells containing a "0" indicate no change compared to System 1. Cells containing a "+" indicate better results than System 1 (e.g., a "+" in weight implies a lighter system). Cells containing a "-" indicate worse results than System 1. Multiple symbols

Table 4.2: Further comparison of fuel system characteristics.

	Weight	**Reliability**	**Cost**
System 1	0	0	0
System 2	-	- -	-
System 3	+	≈ 0	≈ 0
System 4	- -	-	- -

within a cell suggest a greater degree of improvement or decline relative to System 1.

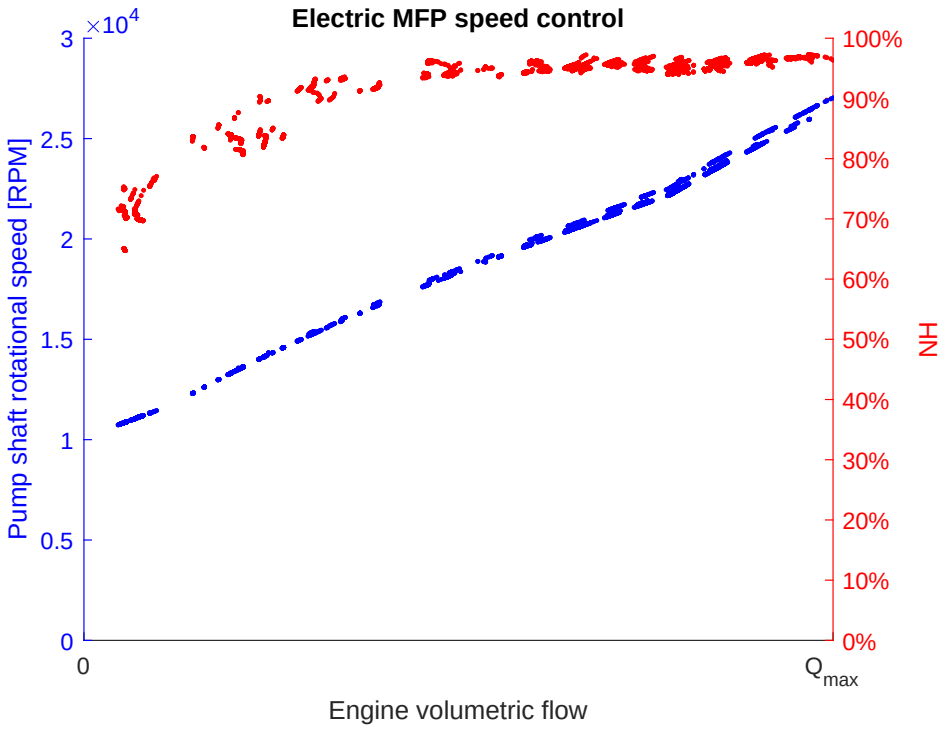

Figure 4.10: Pump shaft speed vs. volumetric flow delivered to the engine for System 4.

5
Discussion

5.1 Discussion of results

This section contains a brief discussion of the results along with important considerations regarding the interpretation of the results, including discrepancies that may affect the results. Test rig limitations and a discussion of the gear pump total efficiency behavior are included. Lastly, possible future work aiming to improve the models are covered.

5.1.1 General findings

Regarding the power usage, System 1 was surpassed by all other systems at IRP and MT, and placed second to last in power usage during FI as can be seen in Fig. 4.1, 4.2, and 4.3. The overall high power usage was expected as a bypass was used to meter the flow. What was not expected, however, was that while the total temperature rise in the system seems to increase with the bypass ratio as can be seen in Fig. 4.7, a majority of the temperature rise during high bypass ratios seems to originate in the LP stage of the MFP, as can be seen in Fig. 4.8. This is due to a low LP stage efficiency at low flow coefficients, coupled with a low volumetric flow rate.

System 3 had a greater power usage than System 1, but only at FI. This is most likely due to an excess pressure buildup at low engine volumetric flows as can be seen in Fig. 4.9. While the driving energy for System 3 was lower than System 1 at IRP and MT, System 3 still required the highest required driving energy over the entire mission, as can be seen in Fig. 4.5. As throttling of the excess pressure lead to a temperature increase, coupled with low centrifugal pump efficiencies at low flow coefficients, System 3 also gave rise to the highest temperature increase at FI. It is however important to note that due to the assumptions and simplifications made in establishing the pump curve behavior of the system, it might be possible to decrease both the temperature rise and power use in the system, by designing pumps with a flatter pump curve (for example by using a partial emission pump in the HP stage), or by placing the BEP further to the left on the pump curves.

System 2 and System 4 both had a superior performance compared to System 1 and System 3. Especially notable for System 4 is the low power usage and temperature increase at FI, as can be seen in Fig. 4.1 and 4.4. This effect can be explained by the ability to control the speed to match the engine requirements. It can be seen in

Fig. 4.10, that the pump rotational speed changes in a manner unlike the change in NH.

While the temperature rise between different systems are large at FI, the overall cooling capacity for a typical mission was similar for all systems, as seen in Fig. 4.6. The differences between the different systems will be larger if the maximum allowed temperature is lowered and/or the inlet temperature is higher if a specific mission need to operate at FI for an extended time period.

If a decrease in temperature rise and power use is deemed important enough to warrant the selection of a new MFP, System 2 and System 4 are most likely superior. However, as can be seen in Fig. 4.2, System 2 is assumed to have a lower reliability, which needs to be addressed before it can be considered as a viable option. Likewise, System 4 is likely heavier due to the additional electric components. In order for this system to be viable, the weight needs to be reduced. This issue might be mitigated if there is already a need to include a large generator in the aircraft, allowing a reduction of the additional weight imposed by the MFP. Furthermore, as System 4 is not driven mechanically it can be placed in the aircraft with greater freedom.

5.1.2 Discrepancies affecting result

As mentioned in Sec. 3.3.3, the mean run time of each test point in the test rig was approximately 2 minutes. Having analyzed the collected data, the HP outlet fuel and bypass temperature was confirmed to having not reached a completely steady state for most test points. This was compounded by the inability to set a representative outlet pressure due to limitations in the test rig. In order to create a model, uninstalled engine test data was used to calibrate the total efficiency of the HP gear pump, with assumed servo flow mass flow rate, temperature behaviors, and fuel properties etc. Discrepancies between the assumptions made and the real-world conditions thus affect the modeled total efficiency of the gear pump.

Another discrepancy can be found in connection to the estimations of the pump curve behavior for System 3 and 4. The centrifugal pump curves consisted of rough estimations. The pump curve used for the System 4 LP stage did not take into account the use of a fuel filter or pump inducer. The high speed of the pump also needs to be evaluated further to ensure that cavitation can be avoided at the chosen operational speeds.

When modeling the pump behavior, the fluid properties used was estimated as the mean values evaluated at the pump inlet and outlet. This assumption is not completely accurate, as the actual equivalent fluid properties, and the change of these properties when passing through the pump are largely unknown.

Lastly, the Joule-Thomson coefficient was determined using data points with a larger population at lower temperatures. The accuracy of the estimation at higher temperatures may therefore be lacking.

5.2 Test rig limitations

Due to unforeseen limitations in the test rig, it was not possible to set an appropriate outlet pressure during the custom MFP rig test. This entailed a need to use uninstalled engine tests to estimate the total efficiency of the gear pump. While this ensured that the overall temperature behavior of the MFP model was reasonably accurate, it may have introduced inaccuracies into the gear pump efficiency model. As this calibration could not be done with alternative systems, it is possible that effects included in the behavior of the gear pump total efficiency are excluded in other models. This error may have been possible to avoid, had it been possible to directly measure the total efficiency of the gear pump during the tests.

Another limitation present in the test rig regards the test rig torque sensor. The sensor returned non-physical and erroneous values; both negative values and unreasonable amplitudes. Attempts to recalculate the torque signal was conducted, without success. It was concluded that a complete recalibration of the sensor need to be performed, which is still yet to be done. Had the torque sensor been in working order, it would have been possible to perform a validation of the power usage and efficiencies derived using temperature measurements.

Lastly, it was not possible to obtain the accuracy of the sensors used in the MFP and engine test rigs. While the data seemed to be of a high resolution, the actual error margin of the data is unknown.

5.3 Gear pump total efficiency curve behavior

A possible explanation for the efficiency behavior seen in Fig. 3.9, is connected to the construction of the pump. The pump uses pressure compensated side plates. In essence, high pressure fluid at the outlet is used to press the side plates against the sides of the gears in order to create a tight seal. As the fuel is of low viscosity, it may be possible to provoke a contact with greater friction by pressing the side plates against the gears with a large force. At high pressure differentials, the side plates are subsequently pressed with a greater force against the gears. With reference to [18], this may induce conditions of insufficient hydrodynamic film load carrying capability. The side plates may thereby impose a braking force, lowering the mechanical efficiency and thus total efficiency of the pump. As the stated total efficiency of the axial piston pumps used in the Saab 35 Draken fighter jet is high, and since this type of pump does not make use of this type of side plates the same type of braking effect may not be present. It may offer an explanation as to why the expected total efficiency using axial piston pumps is greater, even if the fluid used is of low viscosity.

5.4 Future work

More work can be done in multiple areas in order to improve the models. Possible areas of improvement are listed below:

- Conduct new rig tests with a longer run time, in order to ensure steady state conditions. If torque measurements are calibrated, these can be used to validate the estimated efficiencies.

- Obtain more accurate fluid properties, including the Joule-Thomson coefficient for both the fluid used in the test rig, as well as for the fuel used in the engine. This will decrease the error in estimated behaviors.

- Collect better pump curve data, with an emphasis on rotodynamic pumps, taking into account the use of inducers and filters, ensuring pumps can be operated without cavitation. This would include data for partial emission pumps.

- Improve weight, cost and reliability estimations. This will allow for recommendations of systems with greater confidence.

- Include the ABP in the model.

- Assess the transmission requirements using different systems architectures, including transmission sizing.

- Include the pump model in an engine performance model in order to assess the total impact on SFC, available power, etc. of different systems.

6
Conclusion

In this thesis, the task was to model the current fuel system of the RM12 engine operating in steady state conditions, and to identify and model alternative fuel system configurations. The data for the RM12 system has been collected through accessory rig tests as well as from uninstalled engine rig tests at varying operating points. Non-classified and publicly available data has been used to identify and model the alternative fuel system configurations. Below the different investigated issues are covered in order as presented in Sec. 1.4, along with the degree to which the issues have been answered.

- The pumps relevant for use in the RM12 engine fuel system includes: external gear pump, axial swash plate piston pump, radial centrifugal pump, and partial emission pump. The flow rate control methods relevant for use in the RM12 engine fuel system includes: flow control by recirculation, variable displacement, throttling, and speed flow control using an electric motor. To model pumps, pump curves and efficiency curves was used, assuming an incompressible fluid, using fluid properties estimated as the mean of pump inlet and outlet properties.

- An estimation of the energy imparted to the fluid, including heat losses and mechanical transmission losses have been created for the different systems. It has not been possible to directly evaluate other losses, such as heat lost to the environment, however it is assumed that these losses contribute little to the overall energy use. In order to evaluate these losses, more data is needed.

- Fuel systems were modeled at steady state. The final state given a certain input was evaluated by iteratively solving for pressure, temperature and mass flows until convergence.

- Different fuel systems have been evaluated, on the basis of temperature increase, power use, and to a lesser extent weight, cost and reliability. The preferred system largely depends on the operational requirements of the mission, and the results in this thesis can thus be applied to better understand the effect on the operational requirements given different systems.

Bibliography

[1] Donovan, A. B., Roberts, R. A., & Wolff, M. (2015). *Fuel pump trade study for a conceptual design of an integrated air vehicle system.* 13th International Energy Conversion Engineering Conference, Propulsion and Energy Forum. American Institute of Aeronautics and Astronautics. https://doi.org/10.2514/6.2015-4172

[2] Ervestrand, J. (2005). *Förbättrad förbränningsstabilitet i EBK för turbofläktmotor RM12 genom förändrad motorreglering: Improved afterburner combustion stability for turbofan engine RM12 by modified engine control* (Dissertation). Linköping University, Department of Electrical Engineering.

[3] Hansen, L. D., Kucera, G. D., Clemons, J. S., & Lee, J. (1997). *Aircraft gas turbine engine fuel pumping systems in the 21st century.* Journal of Engineering for Gas Turbines and Power, 119(3), 591-597. https://doi.org/10.1115/1.2817025

[4] Rolls Royce. (2005). *The jet engine.* Rolls Royce Technical Publications.

[5] Oba, D., & Gonda, Y. (2014, June). *Fuel system with variable speed pump to improve thermal management ability for aircraft engines.* Proceedings of ASME Turbo Expo 2014: Turbine Technical Conference and Exposition. ASME. https://doi.org/10.1115/GT2014-26809

[6] Li, D., Hang, J., Li, Y., & Dong, S. (2022). *Fuel flowrate control for aeroengine and fuel thermal management for airborne system of aircraft—An overview.* Applied Sciences, 12(1), 279. https://doi.org/10.3390/app12010279

[7] The Engineering ToolBox. (2004). *Orifice, nozzle and venturi flow rate meters.* Retrieved April 3, 2024, from https://www.engineeringtoolbox.com/orifice-nozzle-venturi-d_590.html

[8] Karassik, I. J., Messina, J. P., Cooper, P., & Heald, C. C. (Eds.). (2008). *Pump handbook* (4th ed.). McGraw-Hill. https://www.accessengineeringlibrary.com/content/book/9780071460446

[9] White, F. M. (2016). *Fluid mechanics in SI units* (8th ed.). McGraw-Hill Education.

[10] Williams, L. T. (2022). *Fundamentals of external gear pump design.* Naval Research Lab Washington DC.

[11] Balje, O. E. (1981). *Turbomachines - A guide to design, selection and theory.* John Wiley & Sons, Inc.

[12] Shi, X., & Manring, N. D. (2001). *A torque efficiency model for an axial-piston swash-plate type hydrostatic pump.* Bath Workshop on Power Transmission and Motion Control, London, UK.

[13] Michael, P., Khalid, H., & Wanke, T. (2012). *An investigation of external gear pump efficiency and Stribeck values.* SAE Technical Papers. https://doi.org/10.4271/2012-01-2041

[14] Michael, P. (2014). *An investigation of viscosity effects on axial piston motor efficiency.* In Proceedings of the 2014 STLE Annual Meeting & Exhibition, May 18-21, Disney's Contemporary Resort, Lake Buena Vista, Florida, USA.

[15] Nichols, K. E. (n.d.). *How to select turbomachinery for your application.* Barber-Nichols Inc. Retrieved April 11, 2024, from https://barber-nichols.com/wp-content/uploads/2019/11/how_to_select_turbomachinery_for_your_application.pdf

[16] Karassik, I. J., & McGuire, T. (2012). *Centrifugal pumps* (2nd ed.). Springer. https://doi.org/10.1007/978-1-4615-6604-5

[17] Murray, J. (1969). *High speed pumps for gas turbine engines.* SAE Technical Paper 690743. https://doi.org/10.4271/690743

[18] Morgridge, D., Evans, H. P., Snidle, R. W., & Yates, M. K. (2011). *A study of seal lubrication in an aerospace fuel gear pump including the effects of roughness and mixed lubrication.* Tribology Transactions, 54(4), 657-665. https://doi.org/10.1080/10402004.2011.589963

[19] Manring, N. D., & Fales, R. C. (2020). *Hydraulic control systems* (2nd ed.). John Wiley & Sons. https://app.knovel.com/hotlink/toc/id:kpHCSE0004/hydraulic-control-systems/hydraulic-control-systems

[20] Kothandaraman, C. P., & Rudramoorthy, R. (2011). *Fluid mechanics and machinery* (3rd ed.). New Academic Science.

[21] Gülich, J. F. (2014). *Centrifugal pumps* (3rd ed.). Springer. https://doi.org/10.1007/978-3-642-40114-5

[22] Dick, E. (2022). *Fundamentals of turbomachines.* Springer. https://doi.org/10.1007/978-3-030-93578-8

[23] Thomas, L. (1965). *A forced vortex pump for high speed, high pressure, low flow applications.* SAE International. https://doi.org/10.4271/650502

[24] Li, W. (2024). *A mathematical model for experimental head-flow rate curve of partial emission pumps.* Engineering Perspective, 4(1), 1-6. https://doi.org/10.29228/eng.pers.74533

[25] Edwards, J. T. (2020). *Jet fuel properties.* Air Force Research Laboratory.

[26] Defense Technical Information Center. (1983). *Handbook of aviation fuel properties*. Coordinating Research Council, Inc.

[27] Whillier, A. (1968). *Pump efficiency determination in chemical plant from temperature measurements*. Industrial & Engineering Chemistry Process Design and Development, 7(2), 194-196. https://doi.org/10.1021/i260026a007

[28] Perry, R. H., & Green, D. W. (1984). *Perry's chemical engineers' handbook*. McGraw-Hill.

[29] Parker Hannifin Manufacturing Germany GmbH & Co. KG, Pump & Motor Division Europe. (n.d.). *Axial piston pumps series PVplus – Design series 47*. Parker Hannifin Corporation. Retrieved from https://www.parker.com/Literature/PMDE/Catalogs/Piston_Pumps/PV+/MSG30-3245_UK.pdf

[30] Parker Hannifin Corporation, Hydraulic Pump and Power Systems Division. (2023). *Variable volume piston pumps series PVP*. Parker Hannifin Corporation. Retrieved from https://www.parker.com/content/dam/Parker-com/Literature/Hydraulic-Pump-Division/PVP-Files/PVP_HY28-2662-Catalog.pdf

DEPARTMENT OF MECHANICS AND MARITIME SCIENCES
CHALMERS UNIVERSITY OF TECHNOLOGY
Gothenburg, Sweden
www.chalmers.se

CHALMERS
UNIVERSITY OF TECHNOLOGY